

NASA CR-159,119



3 1176 00156 6042



Materials Sciences Corporation

NASA-CR-159119
19800002899

NASA CR-159119

MSC TFR 1005/0206

DEVELOPMENT OF A REALISTIC STRESS ANALYSIS
FOR FATIGUE ANALYSIS OF NOTCHED COMPOSITE LAMINATES

E. A. Humphreys
B. Walter Rosen
Materials Sciences Corporation
Blue Bell, PA 19422

Contract NAS1-15411

May 1979

NASA

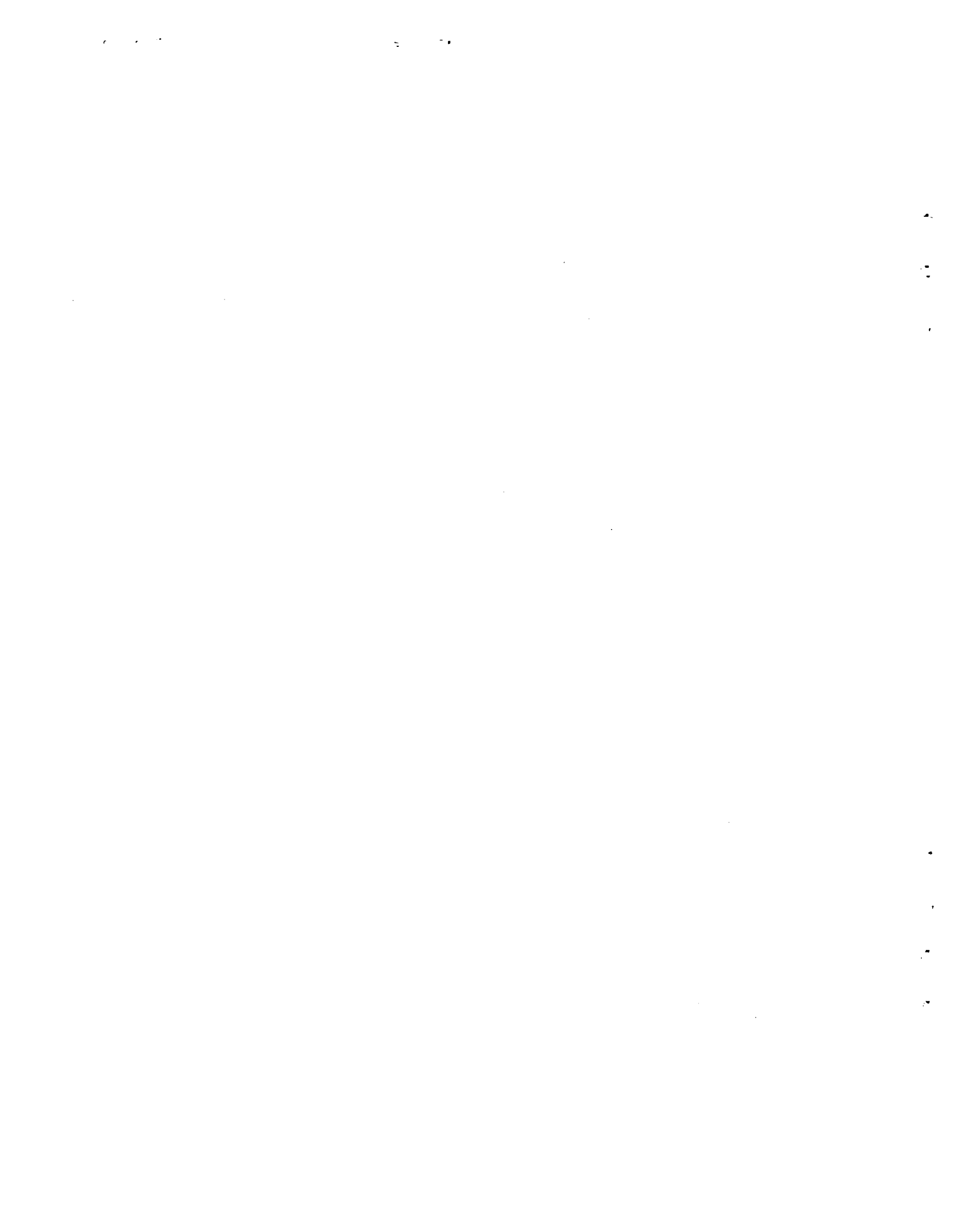
National Aeronautics and
Space Administration

Langley Research Center
Hampton, Virginia 23665
AC 804 827-3966

LIBRARY COPY

NOV 27 1979

LANGLEY RESEARCH CENTER
LIBRARY
HAMPTON, VIRGINIA



DEVELOPMENT OF A REALISTIC STRESS ANALYSIS
FOR FATIGUE ANALYSIS OF NOTCHED COMPOSITE LAMINATES

E. A. Humphreys and
B. Walter Rosen

MSC TFR 1005/0206
Contract NAS1-15411

May 1979

Prepared for:

National Aeronautics and Space Administration
Langley Research Center
Hampton, Virginia 23665

Prepared by:

Materials Sciences Corporation
Blue Bell Office Campus
Merion-Towle House
Blue Bell, Pennsylvania 19422

N80-11146 #

FOREWORD

This report summarizes the work accomplished by the Materials Sciences Corporation under NASA Contract No. NAS1-15411. Dr. G. L. Roderick (US AAMRDL, Langley Directorate) was the NASA Project Engineer, and the authors express appreciation for the technical discussions held with him.

The Project Manager and Principal Investigator for MSC were Dr. B. W. Rosen and Mr. E. A. Humphreys, respectively. Dr. R. L. Ramkumar participated in the early stages of this program. The authors would like to express their appreciation to Dr. Z. Hashin and Dr. M. Newman for their many helpful technical inputs during the course of this program.

Approved by:



B. Walter Rosen
President

The contract research effort which has led to the results in this report was financially supported by the Structures Laboratory, USARTL (AVRADCOM).

TABLE OF CONTENTS

	<u>Page</u>
SUMMARY.	1
SYMBOL LIST.	2
INTRODUCTION	3
STRESS ANALYSIS OF NOTCHED COMPOSITE LAMINATES	5
MODEL REQUIREMENTS	5
FORMULATION OF THE MODEL	5
EVALUATION OF THE MODEL.	8
APPLICATION OF THE MODEL	12
FATIGUE ANALYSIS OF NOTCHED COMPOSITE LAMINATES.	14
FATIGUE METHODOLOGY.	14
FAILURE CRITERION.	15
DEMONSTRATION OF FATIGUE ANALYSIS.	15
CONCLUSIONS.	20
APPENDIX A - COMPUTER PROGRAM DESCRIPTION.	21
APPENDIX B - MEMBRANE AND SHEAR SPRING STRESS ANALYSIS MODEL.	36
APPENDIX C - QUASI THREE-DIMENSIONAL FINITE ELEMENT ANALYSIS	38
REFERENCES	39
TABLES	40
FIGURES.	46

DEVELOPMENT OF A REALISTIC STRESS ANALYSIS
FOR FATIGUE ANALYSIS OF NOTCHED COMPOSITE LAMINATES

E. A. Humphreys and
B. Walter Rosen

Materials Sciences Corporation

SUMMARY

This report describes the development of a finite element stress analysis and its incorporation into an existing fatigue analysis methodology. The fatigue analysis is developed in order to allow for comparisons of various laminate configurations under fatigue loadings.

The stress analysis developed for this study consists of a membrane and interlaminar shear spring analysis. This approach is utilized in order to model physically realistic failure mechanisms while maintaining a high degree of computational economy. The accuracy of the stress analysis predictions is verified through comparisons with other solutions to the composite laminate edge effect problem. The first comparison is with an existing finite difference solution for a $[\pm 45]_S$ laminate. The second comparison is with quasi three-dimensional brick finite element results for a $[\pm 30/90]_S$ laminate. The present model is shown to yield satisfactory results.

The stress analysis model is then incorporated into the existing fatigue analysis methodology and the entire procedure computerized. A fatigue analysis is performed upon a square laminated composite plate with a circular central hole. The laminate orientation is $[0_2/\pm 45]_S$. Resulting damage initiation and growth is demonstrated at 1000 and 10,000 fatigue cycles. In addition, the strength of the notched laminate is calculated for the static case (one cycle) and at 10,000 fatigue cycles. These strength predictions also include damage growth predictions. A complete description and users guide for the computer code FLAC (Fatigue of Laminated Composites) is included as an appendix to the report.

SYMBOL LIST

A	- Area;
b	- Laminate half width;
c	- Notch radius
E_{ii}	- Extensional modulus of elasticity;
F	- Force;
G_{ij}	- Shear modulus;
H	- Laminate half thickness;
h_o, t	- Ply thickness;
I	- Bending moment of inertia;
L	- Beam length;
LX	- Laminate length;
N	- Number of fatigue cycles;
NINT	- Number of ply interfaces
r	- Radial coordinate
u_i, U_i	- Displacements in the i-direction;
Δ	- Displacement;
ν_{ij}	- Poisson's ratio (strain in j-direction due to load in i-direction);
σ_{ij}, σ	- Stress;
σ_u	- Ultimate static strength;
σ_∞	- Far field stress;
σ_A^+	- Lamina axial tensile strength;
σ_A^-	- Lamina axial compressive strength;
σ_T^+	- Lamina transverse tensile strength;
σ_T^-	- Lamina transverse compressive strength;
τ	- Lamina in-plane shear strength and interlaminar shear strength.

INTRODUCTION

The use of laminated composites as primary structural materials has generated the need to characterize the response of these materials under all anticipated environments. Thus, the need to understand the fatigue and fracture characteristics of the material is primary. However, to define completely, through experiment, the fatigue characteristics of the multitude of laminates available to the designer would be prohibitively costly. Because of this, considerable effort has been directed toward developing an analytical methodology that will predict the relative merits of composite laminates subjected to fatigue loading, and thereby substantially reduce the number of experiments required.

This effort was initiated in the study reported in reference 1 with the development of a methodology for predicting crack growth and ultimate failure of a notched composite laminate under fatigue loading. The analysis was based upon the premise that the fatigue characteristics of an arbitrary laminate can be predicted utilizing experimental lamina properties. The stress analysis involved was basically a shear lag analysis with certain approximations made to the stresses in various regions parallel to the loading directions, emanating from the edges of a through-the-thickness hole.

In reference 2, an effort was made to correlate the predictions of reference 1 with experimental data as well as to generate the data necessary for the model developed in reference 1. In addition, an analysis was made in which the spatial variation of material properties was allowed. This was done to reflect the substantially higher stresses and therefore damage, in the region near the notch.

In reference 3, the model was further expanded to account for interlaminar effects. In the region closest to the notch, the laminate was modeled as individual laminae. The principal drawback of the model at this stage was the complexity involved in tracking various multiple damage sequences. In addition, the failure mode predictions being made were becoming much more detailed than was warranted by the nature of the stress analysis.

Therefore, a new stress analysis was required that could be used for failure prediction while maintaining the fatigue concepts of the earlier models.

The primary objective of the current study was to incorporate a finite element stress analysis into the fatigue analysis model. In order to maintain computational economy, a two-dimensional membrane and shear spring finite element model was used to predict in-plane and interlaminar stresses, respectively. Pertinent features of the stress analysis can be found in the section "Stress Analysis of Notched Composite Laminates".

The analysis procedure has been used to predict the residual strength of a notched composite laminate at various times in the laminate's fatigue lifetime. In addition, damage growth was predicted as it grew in the laminate with the number of fatigue cycles.

The fatigue analysis methodology has been incorporated into a computer code, FLAC (Fatigue of Laminated Composites). A complete description and users guide to the code can be found in Appendix A.

STRESS ANALYSIS OF NOTCHED COMPOSITE LAMINATES

The principal goal of this study was to develop a finite element stress analysis of notched laminates, and to incorporate that analysis into the fatigue analysis procedure developed in references 1, 2, and 3.

MODEL REQUIREMENTS

The stress analysis procedure must be capable of providing a realistic stress distribution including both in-plane and interlaminar stress components. The procedure must incorporate failure criteria which can utilize the computed stresses to predict local damage. Further, there must be provisions to modify the model to reflect the changes caused by local damage, in order to permit prediction of subsequent damage.

The need for realism of stress predictions motivated the use of finite element models. The need to treat a large number of damaged or failed elements requires that attention be paid to computational economy. The need to assess the effects of local damage requires the use of physically based failure criteria.

The failure criteria used are described in Appendix A. These criteria treat three different types of failure, namely: a matrix-dominated in-plane failure; a fiber-dominated in-plane failure; and an interlaminar failure. Only the in-plane stress components are treated as influencing the in-plane failure mechanisms, and only the interlaminar shear and normal forces are treated as influencing the interlaminar failure. Because each stress component influences at least one failure mode, a three-dimensional stress analysis was suggested.

FORMULATION OF THE MODEL

Initially, a three-dimensional brick finite element analysis was considered to be the desirable choice. Effort was devoted to the modification of a finite element analysis code, HEX, (ref. 4) and to development of models for stress analysis of various laminate configurations. After making the HEX code operational on our

computer system, and running several sample analyses, the cost of executing HEX was found to be prohibitive. Further investigation showed the cost of other finite element codes with three-dimensional bricks would also be prohibitive. In order to maintain a realistic stress analysis and to develop a cost-effective computer code for the fatigue analysis, a simplified model was adopted. This new approach consisted of modeling the balanced, symmetric composite laminate ply by ply as orthotropic membrane elements in a state of plane stress, and two-dimensional beam elements connecting the plies at the nodal points carrying the interlaminar forces. The routines and procedures for the displacement formulation, finite element stress analysis have been adapted from the SAP IV finite element analysis code (ref. 5). In the finite element model, only one-half of the plate thickness need be modeled due to symmetry conditions inherent in the balanced symmetric laminates.

The beam elements acting as shear springs in the model are configured such that they have a moment of inertia, I , which yields the appropriate force-displacement relationship. The relation for this geometric property can be found in Appendix B.

The model described does not predict the interlaminar normal forces directly. However, the stress equilibrium relations,

$$\sigma_{ji,j} = 0 \quad (1)$$

enable the interlaminar normal stresses to be approximated from the interlaminar shear stresses. The relation in rectangular coordinates is:

$$\sigma_{zz} = - \frac{\partial}{\partial x} \int \sigma_{xz} dz - \frac{\partial}{\partial y} \int \sigma_{yz} dz. \quad (2)$$

This equilibrium equation can be readily modified for use with the membrane and shear spring stress analysis model. First, the integrals through-the-thickness of the plate must be replaced with summations. Thus,

$$\int \sigma_{xz} dz = \sum_{I=1}^{Nint} \frac{F_x^{(I)}}{A} t^{(I)} \quad (3)$$

and

$$\int \sigma_{yz} dz = \sum_{I=1}^{Nint} \frac{F_y^{(I)}}{A} t^{(I)} \quad (4)$$

where

1. the summation is carried out from the lower surface of the plate (not the mid surface),
2. the summation is carried out at each spring location in the X-Y plane,
3. $F_x^{(I)}$ and $F_y^{(I)}$ are the shear spring (beam) forces in the X and Y coordinate directions, respectively, at interface I, at the same spring location in the X-Y plane,
4. $t^{(I)}$ is the length corresponding to the beam at interface I, and
5. A is the area corresponding to the shear springs at the point in the X-Y plane.

Once these summations are performed at each of the shear spring locations in the X-Y plane, the partial derivatives are carried out in both the X and Y coordinate directions for a given value of Z (corresponding to an interface). These derivatives are evaluated using finite difference relations which yield a numerical approximation of the slope of the previously mentioned summations in both the X and Y coordinate directions. As will be seen in the following section, the interlaminar normal stresses obtained by this method do not agree well with results available in the literature.

This membrane and beam model is described in further detail in Appendices A and B. This model has the advantage that in-plane and interlaminar failure criterion are applied separately to different elements. When a failure occurs, appropriate stiffnesses of the damaged element are reduced. For the interlaminar failure, the beam bending stiffness is reduced. For the in-plane matrix-

dominated failure, the membrane axial shear and transverse extensional stiffnesses are reduced. For fiber-dominated failure, all membrane stiffnesses are reduced. After these stiffness reductions, the stiffness matrix is modified and the stress analysis proceeds in an incremental fashion.

EVALUATION OF THE MODEL

To verify that the membrane and shear spring analysis yields a realistic stress prediction, comparisons were made with two other stress analyses. First, a comparison was made with finite difference results for the edge effect problem (ref. 6). The laminate orientation compared was $[\pm 45]_s$. Secondly, a comparison was made with a quasi three-dimensional finite element analysis of the same edge effect problem, but comparing a different laminate $[\pm 30/90]_s$. The quasi three-dimensional analysis was provided by Dr. G. L. Roderick, NASA Langley, and is described in Appendix C.

The shear spring and membrane stress analysis model used in both of the previously mentioned comparisons had identical geometries in the plan form (fig. 1, X-Y plane). The models differed in both the number of plies and in the thickness of the plies.

For the analysis of the $[\pm 45]_s$ laminate, the ply thickness used was $b/8$ as was used in reference 6. For the model used to compare results with the quasi three-dimensional analysis, the ply thickness used was $b/32$, as this was used by Dr. Roderick.

Both the finite difference analysis of reference 6 and the quasi three-dimensional analysis assume that the laminate is infinite in the loading direction (X-direction). In order to simulate this, seven rows of membrane elements and eight rows of shear springs are used in the loading direction in the present analysis. The membrane and interlaminar stresses are evaluated in a central X-coordinated location (St. Vennant's Principle).

The predictions of the $[\pm 45]_s$ laminate stresses are plotted in figure 2. The material properties used for this laminate, and for the $[\pm 30/90]_s$ laminate are those used in reference 6 and are listed in table 1.

Comparing the stresses depicted in figure 2, a good correlation between the two analysis procedures can be seen in some of the stress components. The σ_{xx} stresses as predicted by finite difference and those predicted with the present analysis are nearly identical. Comparing the σ_{xy} and σ_{xz} stresses, a fair correlation can be seen. The present solution produces similarly shaped distributions, but with somewhat reduced magnitudes. Here, the comparisons are not as good as with the σ_{xx} stresses. The stresses are still sufficiently accurate for making the qualitative comparisons between laminates, even though the ability to predict quantitative residual strengths may be restricted. The σ_{yy} stresses of the present study are similar to those of reference 6, but there are differences between them. Both the σ_{yy} and σ_{xy} stresses do satisfy the stress-free boundary conditions at the free edge ($Y/b = 1.0$).

A drawback in using the above laminate for comparison purposes is that the $[\pm\theta]_s$ orientation produces very small σ_{yz} and σ_{zz} stresses. Because of this, the second laminate chosen for comparison was a $[\pm 30/90]_s$ configuration. The interlaminar stresses as predicted by the quasi three-dimensional finite element analysis as those of the present study are depicted in figures 3, 4, and 5.

In figure 3, the interlaminar shear stresses at the $(-30/90)$ ply interface are presented. The σ_{xz} stresses as predicted by both finite element analyses are very similar, both in magnitude and distribution. The σ_{yz} stresses are also similar throughout much of the laminate. However, as Y/b approaches 0.95, the quasi three-dimensional analysis predicts a reversal in the slope of the σ_{yz} curve while the present analysis does not. Thus, the quasi three-dimensional analysis predicts stresses that approach the stress-free boundary condition at the free edge, while the shear spring and membrane analysis does not.

In figure 4, the comparison of interlaminar shear stress predictions of the two analyses indicates a good correlation of σ_{xz} stresses at the $(+30/-30)$ ply interface. Comparing the σ_{yz} shear stresses, the discrepancy noted for the $(-30/90)$ interface appears again. The stress-free boundary condition at $Y/b = 1.0$ is

not satisfied continuously by the membrane and shear spring analysis. At both ply interfaces the σ_{yz} stresses, predicted by the present analysis, start to build in magnitude with increasing Y/b . However, they fail to reverse to zero at the free edge ($Y/b = 1.0$).

This lack of reversal in stress near the free edge causes significant problems when the interlaminar normal stress is computed using the stress equilibrium relations (eqns. 1,2). This is clearly demonstrated in figure 5, which represents the σ_{zz} stresses at the two-ply interfaces.

In figure 5, it can be seen that both analyses predict that the normal stress is compressive as it develops with increasing Y/b . The quasi three-dimensional analysis predicts that the normal stresses are non-zero further away from the laminate edge than the present analysis. The normal stress is computed directly from σ_{yz} (eqn. 2), and therefore it becomes non-zero as σ_{yz} does. The quasi three-dimensional solution predicts non-zero normal stress further into the laminate than it predicts σ_{yz} stresses. In this regard, perhaps the present analysis is superior to the quasi three-dimensional analysis. However, the quasi three-dimensional analysis predicts reversed normal stresses when the membrane and shear spring analyses do not. It is known that the normal force over the region must vanish such that:

$$\int_{-\infty}^{\infty} \int_{-b}^b \sigma_{zz} \, dy \, dx \quad (5)$$

Since the analysis requires no variation of stress with the X-coordinate and the laminate is symmetric, equation 5 can be reduced to:

$$\int_0^b \sigma_{zz} \, dy = 0 \quad (6)$$

Hence, the σ_{zz} stresses plotted must have equal areas of tension and compression. Here, clearly, the prediction of the normal stress in the present analysis is invalid from an equilibrium standpoint.

Again considering the normal stresses depicted in figure 5, it is apparent that neither solution procedure produces physically attractive stresses at the free edge. The present analysis requires that a partial derivative be evaluated (eqn. 2) at various spring locations to predict the normal stresses. This differentiation is carried out using a finite difference scheme. Since the σ_{yz} stress components do not satisfy the stress free boundary conditions at $Y/b = 1.0$ (figs. 3,4) and must therefore be incorrect there, the normal stress cannot be predicted accurately at this point. It is possible to satisfy equilibrium by including a discontinuous jump in the σ_{zz} stress at the free edge in the form of a delta function.

The normal stresses predicted by the quasi three-dimensional analysis at the (+30/-39) ply interface are oscillating between large positive and negative values. This effect also appears to be physically unrealistic.

An attempt was made to force satisfaction of the stress free boundary condition of σ_{yz} in the shear spring and membrane analysis by removing the stiffness of the shear springs in the Y-direction at the free edge. This effort was successful only in shifting the σ_{yz} curve inward by one beam.

As it had become apparent that neither solution method was capable of producing a satisfactory normal stress in the vicinity of the free edge, their calculation was omitted from the computerized analysis. Provisions were made in the program for the inclusion of the normal stresses should a satisfactory method of obtaining them be devised.

An adjustment was made to the model in order to determine how sensitive the interlaminar stress predictions were to changes in the shear spring properties. The modification consisted of reducing the shear spring stiffness by a factor of 4. Also, this adjustment would hopefully reveal any inherent over-stiffnesses in

the model. This modification produced stresses that were slightly different, but not discernably better. The interlaminar shear stresses as predicted by the modified model are shown in figures 6 and 7.

APPLICATION OF THE MODEL

The stress analysis developed here has been shown to yield results comparable to both the quasi three-dimensional analysis and finite difference solution for balanced, symmetric composite laminates. The laminate selected for the fatigue analysis was a $[0_2/\pm 45]_S$ graphite epoxy notched plate. The elastic properties selected correspond to the G/E system T-300/5208, and are listed in table 2.

The finite element model developed for the stress analysis of notched composite plates is shown in figure 8. The model extends away from the notch, a distance of three notch radii. This distance allows for the three-dimensional state of stress to degenerate into a two-dimensional state within the confines of the model.

Hoop stresses around the notch, as predicted with the current stress analysis model, are shown in figure 9. The stresses presented are predicted at the centroids of the first row of elements. The stresses plotted have been normalized with respect to the far field stress, σ_∞ . The most interesting feature of these stresses is that in the 45° and -45° plies the maximum stress concentration does not occur perpendicular to the loading direction. The peak stress values are slightly to either side of $\theta = 90^\circ$. Another pertinent feature is that the 0° plies have stresses so similar that the differences do not show on the scale of the figure.

The hoop stresses are plotted radially in figure 10. Here, the rapid increase in hoop stress as the ratio r/c decreases to 1.0 is clearly demonstrated. As in the previous figure, the 0° plies are carrying the great majority of the load, as expected due to their much higher stiffness.

In figure 11, the interlaminar shear component, $\sigma_{\theta z}$, is plotted as a function of θ at the edge of the hole. Here, the three curves correspond to the three ply interfaces, 0/0, 0/45, and 45/-45. The largest magnitude, and greatest fluctuation, occurs at the 0/45 interface. This is, of course, due to the relatively large difference in properties between the 0° plies and the rotated $\pm 45^\circ$ plies. It is again interesting that the stresses are not symmetric about $\theta = 90^\circ$.

The $\sigma_{\theta z}$ stress components plotted radially are shown in figures 12, 13, and 14 at the 0/0, 0/45, and 45/-45 ply interfaces, respectively. The angle chosen for the radial stress plots corresponds to the maximum negative value for each interface at the hole edge. The three curves all reach a maximum positive value at $r/c = 1.2$. The peak positive values follow the negative hole edge values in that the 0/45 interface produces the largest value. It can be seen that in the three figures the $\sigma_{\theta z}$ stresses vanish at $r/c = 2.0$, thus supporting the earlier statement that the three-dimensional stress states exist entirely within the model.

Figures 15 and 16 represent the in-plane radial stress, σ_r , and the in-plane shear stress, $\sigma_{r\theta}$, respectively. For both of these in-plane stresses the predictions in the $\pm 45^\circ$ plies appear to be satisfying the stress-free boundary conditions while the 0° ply stresses do not.

The stress distributions predicted by the present analysis for the notched plate have been shown to be reasonable both in shape and in magnitude. Certain of the stress-free boundaries have been met while others have not, as was the case with the infinite coupon edge-effect solutions. The present analysis has also been shown to yield results which compare very favorably with the quasi three-dimensional analysis and with the finite difference solution of reference 6 for the edge effect problems shown. Therefore, the shear spring and membrane stress analysis model has been adopted for inclusion in the fatigue analysis methodology. However, it should be noted that the present understanding of interlaminar normal stresses is incomplete.

FATIGUE ANALYSIS OF NOTCHED COMPOSITE LAMINATES

The primary goal of the current study was to develop a computer code for fatigue analysis of notched composites. This code should provide the capability to assess relative merits of different laminates at the preliminary design stage. The approach taken was to incorporate a finite element stress analysis, described in the previous section, into a fatigue analysis methodology developed in references 1, 2, and 3. The fatigue analysis, including the elemental failure criteria, is briefly described here.

FATIGUE METHODOLOGY

The underlying philosophy of the fatigue methodology can be described as residual laminate strength and stiffness degradation due to material wearout. Hence, the methodology describes a process whereby the reduction of a laminate's residual strength when subjected to fatigue loading is due to an accumulation of localized damage. In a notched composite laminate this damage is most pronounced in the region of high stress concentration near the notch. The method used for predicting this damage considers the laminae to be homogeneous, orthotropic materials. Thus, lamina and interlaminar properties need to be determined experimentally. For the purposes of the fatigue analysis, one-dimensional strengths as functions of both the number of fatigue cycles and the fatigue stress must be measured. These data, along with failure criteria and stresses predicted with the model described in the previous section, can be used to predict the minimum load required to cause a localized failure (least failure load). By systematically changing the properties of damaged or failed elements in the stress analysis model and predicting new least failure loads, the residual strength of the laminate and damage growth to failure can be predicted. By utilizing the experimentally determined laminae residual strengths, the process can be carried out at various numbers of fatigue cycles and thus predict the notched laminates damage growth and residual strength at the fatigue stress level. While it is known that the damage growth and

residual strength degradation are continuous phenomena, their calculation must be carried out at discrete intervals in order that the analysis be tractable.

FAILURE CRITERION

In order to predict localized elemental failures culminating in the laminate failure, an appropriate failure criterion must be utilized. For this study a criteria developed in reference 7 is used. The failure model is particularly well suited for use in this study due to the ease in which it can be separated for in-plane and interlaminar failure predictions. In effect, the model as used contains three criteria: a fiber failure criterion; an in-plane matrix failure criterion; and an interlaminar failure criterion. The fiber and in-plane matrix modes are utilized in conjunction with the membrane element stresses while the interlaminar mode is used with the shearing stresses produced in the beam elements and interlaminar normal stresses. The forms of these failure criterion are given in table A-1.

DEMONSTRATION OF FATIGUE ANALYSIS

For the purposes of demonstrating the capability of the fatigue analysis methodology and the computerized analysis, a $[0_2/\pm 45]_s$ square plate with a central, circular notch was examined numerically under fatigue loading conditions. The laminate static stress distributions, stress analysis model, and elastic constants were discussed in the previous section, "Stress Analysis of Notched Composite Laminates".

As was mentioned previously, the fatigue analysis required one-dimensional strengths as functions of both fatigue stress and the number of fatigue cycles. However, this information does not exist in the literature in complete form. For this reason, the data used in the present study have been largely generated from a single set of residual strength curves found in reference 8. In order to obtain consistency among the residual strength curves as generated, certain data points were taken from constant amplitude fatigue life data in reference 9. Had actual residual strength

data been available, it would have been necessary to use an appropriate curve fitting technique to match the computer program input parameters to the data. The complete set of curves used in this study are shown in figures 17 through 21. It should be noted that for the present study it has been assumed that the in-plane and interlaminar shear properties are identical and thus only one figure is presented for shear data (fig. 21).

For the demonstration analysis the fatigue load used corresponded to a far field stress, σ_{∞} , of 103 MPa. This load corresponds to approximately one-half of the static ultimate strength of the notched laminate. The load required to produce ultimate failure and the first localized failure were predetermined using the computerized analysis. A load of 103 MPa did not cause any damage in the static case.

The value used to replace the moduli of failed elements (REDMOD in the program input) was 689 KPa. Therefore, the reduced modulus value corresponded to a reduction of at least 99.99% for all static moduli. This reduction effectively removed the failed elements from the model without causing any ill-conditioning within the global stiffness matrix.

In the computerized analysis a provision has been included which allows a reduction in the number of iterations required to produce laminate failure. A decimal fraction (labelled TOLER in the program) is input into the program and is used in a comparison between the failure load of each element and the least failure load in the model at each iteration. The comparison states that if

$$\frac{\text{Elemental Failure Load} - \text{Least Failure Load}}{\text{Least Failure Load}} \leq \text{TOLER}$$

then the element has failed at this iteration. For the present study the input value of TOLER was 0.10. With this value, 12 iterations were required to produce fiber failure in the notched laminates at N=1. Hence, 12 was the maximum number of iterations used for each of the three fatigue increments run (N=1, N=1000, and N=10,000).

Another provision included in the computerized analysis causes the residual strength calculations to cease whenever the least failure is reduced from one iteration to the next. For the demonstration analyses, this provision was over-ridden with an input parameter (LOVRD). This caused the solution to proceed through all 12 residual strength iterations without regard to the least failure load.

The cumulative in-plane and interlaminar damage predicted at a load of 179 MPa and $N=1$ in the $[0_2/\pm 45]_S$ notched laminate is depicted in figures 22 and 23. The in-plane damage produced in the membrane elements is shown in figure 22, while the interlaminar damage predicted for the beam elements is shown in figure 23.

As shown in figure 22, the damage within the 0° plies is symmetric about a line perpendicular to the loading direction. A comparison with figure 9 shows the damage occurring to either side of the peak $\sigma_{\theta\theta}$ stresses in the 0° plies. This can be readily explained, as the peak $\sigma_{\theta\theta}$ stresses are aligned in the fiber direction of the 0° plies where the strength is highest. At points to either side of the peak $\sigma_{\theta\theta}$ stresses, however, the fiber orientation no longer coincides with the stress, therefore the strength is reduced and damage is predicted. In both the 45° and -45° plies, however, the damage shows a marked preference for opposite sides of a perpendicular to the loading direction. This is consistent with the stresses of figure 9, where the circumferential stresses in these plies are not symmetric about $\theta = 90^\circ$. In all four of the plies the damage is occurring predominantly in the region perpendicular to the load.

The interlaminar damage in figure 23 is greatest at the 0/45 ply interface. In figure 11, the interlaminar shear stress, $\sigma_{\theta z}$, is maximum at the 0/45 ply interface, thus first failure was anticipated at this interface. As the 45/-45 ply interface has lower stresses, one would expect less damage to be present.

In figures 24 and 25, damage in the laminate at failure, 226 MPa, is depicted. The damage shown is considered to correspond to laminate failure as fiber failure has occurred in the 0° ply element adjacent to a perpendicular to the loading (shaded areas in

the figure). In these figures the damaged regions can be seen to have grown significantly with respect to the results at 179 MPa. An interesting feature is that the damage in the 0° plies is no longer symmetric, indicating that the unsymmetric ±45° ply damage and the interlaminar damage has changed the stress distribution significantly. The interlaminar damage can be seen to have grown with the increased load, also.

One item which cannot be depicted in the figures is that in accumulating the local damage shown in figures 21 through 25, the two 0° plies always failed simultaneously. This is consistent with the stresses plotted in figures 9 through 16, where the 0° ply stresses were nearly identical to each other. In addition, no damage has occurred at the 0/0 ply interface. This is true for all of the results to be presented and is consistent with the stresses described previously where this interface produced the lowest interlaminar shearing stresses.

In figures 26 and 27, damage accumulated after 1000 cycles is depicted. Here, neither of the 0° plies have suffered any damage. The 45/-45 ply interface has also accumulated no damage. In the 45° and -45° plies, as well as the 0/45 ply interface, however, damage is present. The damage is seen to be progressing similarly to the damage at N=1, though at lower load levels, as expected.

In figures 28 and 29, the cumulative damage at 186 MPa and 1000 fatigue cycles at 103 MPa is presented. The total load of 186 MPa corresponds to the load in figures 22 and 23. Comparing the four figures, it can be seen that at 1000 fatigue cycles more damage is present in the -45° ply. In the 45° ply, however, the reverse is true, indicating that the growing damage was re-distributing the load within the notched plate. In addition, after 1000 cycles the different damage states in the 0° plies indicates that the 0° plies have different stresses.

In figures 30 and 31, damage accumulated through 10,000 cycles at 103 MPa is depicted. When these two figures are compared with figures 26 and 27, the damage can be seen to have encompassed an additional 45° ply element, while damage growth in the

other plies and interfaces has ceased. Consequently, the majority of highly stressed elements apparently had failed at 1000 cycles. Due to the nature of the lamina residual strength data (figs. 17-21) the highly stressed elements will degrade much more rapidly than the elements with lower stresses. Thus, after the highly stressed elements have failed, it may take very many additional cycles to produce further damage. In fact, the damage growth may cease entirely if the stress redistribution reduces the stress concentrations below the level at which material degradation occurs.

In figures 32 and 33, the damage corresponding to laminate failure (fiber failure [shaded area] has occurred in the 0° plies) is shown. The load required to produce failure at 10,000 cycles was 208 MPa. The load required to produce laminate failure in the static case (N=1) was 226 MPa (figs. 24,25). The reduction in laminate strength at 10,000 cycles amounts to 8%. This strength reduction was expected and is due to the material strength degradation with increasing fatigue cycles.

The fatigue analysis has demonstrated the capabilities of the fatigue methodology and the computerized analysis procedure. Damage initiation and growth both in the residual strength calculations and at the fatigue load have been demonstrated. In addition, reduction in laminate residual strength with increasing fatigue cycles has been predicted with the current analysis. Thus, the goals of the current study have been accomplished.

CONCLUSIONS

In this study a finite element stress analysis model was developed and incorporated into an existing fatigue analysis methodology. The stress analysis model was verified through correlation with existing laminate stress predictions. The fatigue analysis was then programmed to provide a tool for making comparisons of various composite laminates under fatigue loadings.

The capabilities of the fatigue analysis were demonstrated by performing a fatigue analysis upon a notched laminated plate.

The stress analysis model developed consisted of a membrane and shear spring analysis. This model was chosen, instead of a three-dimensional brick finite element model, in order to be able both to analyze the multiplicity of physically realistic failure modes and to achieve computational economy. The accuracy of the model was demonstrated by comparing results with both a finite difference solution and a quasi three-dimensional finite element analysis. The shear spring and membrane model was shown to compare very favorably with these other solution procedures and thus its accuracy was demonstrated.

The sample analysis of a notched composite laminate demonstrated the ability to calculate damage initiation and growth and residual strength of notched composites under cyclic loads.

The principal limitation of the current study is the absence of any attempt to correlate the analytically predicted fatigue behavior with experimental data. To make this correlation, lamina data are required for input to the computerized analysis and laminate data are required for the fatigue prediction comparisons.

These experimental data would then allow the experimental-analytical correlations necessary for the full verification of the fatigue analysis model.

APPENDIX A
COMPUTER PROGRAM DESCRIPTION

The computer code FLAC (Fatigue of Laminated Composites) performs an analysis of a balanced symmetric composite laminate subjected to constant amplitude fatigue load with the stress ratio equal to 0.0 or -1.0. The program consists of a linear elastic finite element stress analysis (taken from SAP IV, ref. 5) merged with a failure analysis and a fatigue analysis methodology.

The fatigue methodology is depicted in the flow chart of figure A-1. As in any analysis program, the first step is the input of the model definition. The stress analysis model is comprised of orthotropic membrane elements, acting in a state of plane stress, to carry the in-plane lamina loads. Connecting the laminae, carrying the interlaminar loads, are beam elements acting as shear springs. The flexural stiffnesses of the beams must be formulated such that they yield the proper force-displacement relation.

The force-displacement relation for relative displacement of two adjacent plies is:

$$F = \Delta \frac{AG}{t} \tag{A-1}$$

where

- Δ is the relative deflection,
- F is the interlaminar shear force,
- A is the planar area,
- t is the ply thickness, and
- G is the interlaminar shear modulus.

In the beam elements, the moment of inertia is adjusted such that they yield the same stiffness as in eqn. A-1. The beam elements are prescribed in the model to have no rotation at either end. Thus, the force-displacement relation is:

$$F = \frac{12EI}{L^3} \Delta \tag{A-2}$$

where

E is the Young's modulus of the beam material,
I is the flexural moment of inertia,
L is the beam length, and
F and Δ are as in eqn. A-1.

Since L and t are the same quantity, and because it is necessary to match the stiffnesses of eqn's. A-1 and A-2, one obtains the relation:

$$\frac{12EI}{t^3} = \frac{AG}{t} . \quad (A-3)$$

This can be rearranged to yield the proper moment of inertia for the problem:

$$I = \frac{AGt^2}{12E} . \quad (A-4)$$

Lamina fatigue data are input with the elastic material constants for both element types. The loads input need not be unit loads but all predictions of strength, and the maximum fatigue load are keyed to them and are actually ratios with respect to the input loads.

After the elastic solution is obtained, the lamina stresses are used in a failure criteria. A minimum load to produce failure is predicted for each element and then the least of these is determined. The failure criterion were developed in reference 7 and are summarized in table A-1. The least failure load is compared to each of the other failure loads. All elements whose failure load falls within a certain input tolerance of the least failure load (ratio of the difference of the least failure load minus the elemental failure load divided by the least) are assumed to have the least failure load. This causes all such elements to fail at the same load.

The least failure load is then compared to the maximum fatigue load. If the load predicted is the first to exceed the fatigue load, the stresses, global stiffness, load vector, stress recovery matrices, and a vector indicating which element failed previously are saved for use at the next fatigue cycle increment.

The laminate is then checked for a global failure. If laminate failure has not occurred, the analysis proceeds with the residual strength calculation. The elements which have failed have negative stiffness and stress recovery information computed. The negative stiffnesses are added into the existing global stiffness and the negative stress recovery information is added to the existing stress recovery matrices. This process, in effect, removes the failed elements from the model.

The new model, which does not have the previously failed elements in it, is then subjected to the applied loading, a new elastic solution is obtained and least failure load predicted. The process continues until laminate failure is predicted. This failure corresponds the residual strength of the laminate at the current fatigue cycle increment.

Laminate failure is defined as occurring when the least failure load decreases from one residual strength increment to the next. If the laminate has failed, the solution proceeds to the next fatigue cycle increment.

When starting the next fatigue increment, stiffness degradation is assumed not to occur. Thus, the stress distribution at the previous fatigue increment can be used as the starting point for the current increment. The information saved as the failure load increased past the fatigue load at the previous fatigue increment is retrieved. The elemental strengths are modified as a function of the fatigue load stresses of the previous fatigue cycle increment and the current number of cycles.

This strength adjustment is carried out with the use of residual strength degradation curves for the laminae. The form of these curves, and the strength reduction formulation are shown in figure A-2. The curves of figure A-2 must be input for

longitudinal tension and compression, transverse tension and compression, and shear for the membrane elements. The beam elements require input of residual strength curves for both interlaminar normal tension and compression, and interlaminar shear. The data input consists of the ultimate static strength, the tangency point A, and the coefficient B.

The magnitude of the reduction in strength is interpolated linearly between σ/σ_u values. The reduction calculated is for each increment of fatigue cycles, not for the entire number of fatigue cycles. These incremental reductions are applied to cumulative strengths. Thus, the process is similar to a Miner's Rule type of prediction where the fatigue life consumed is computed as a sum partial lives used.

The various routines used in the program are listed in table A-2 along with a brief description of their functions.

PROGRAM USERS GUIDE

Note: The stress analysis model incorporated into FLAC was taken largely from an existing finite element analysis (SAP IV) code. In order to expedite the development of FLAC, some of the capabilities of SAP IV were retained even though they do not apply to the fatigue analysis. Therefore, certain input parameters for FLAC must be input as specific values. These parameters are throughout the FLAC input.

I. PROGRAM CONTROL DATA

<u>Card 1</u>	<u>Title Card</u>	<u>12A6</u>
---------------	-------------------	-------------

<u>Columns</u>	<u>Contents</u>
1-72 HED(12)	Program Title Card

<u>Card 2</u>	<u>Program Control Card</u>
---------------	-----------------------------

<u>Columns</u>	<u>Contents</u>
1-5 NUMNP	Number of nodes
6-10 NELTYP	= 2
11-15 MODEX	Solution Mode, = 1 for data check = 0 for execution
16-20 MAXFAT	Maximum number of fatigue increments
21-25 MAXRES	Maximum number of residual strength increments
26-30 IRST	Restart Code = 0 no restart or data save = 1 save data for later restart = 2 restart = 3 restart and save data for restart later

31-35 LOVRD

Load override = 0, no effect
= 1, disables residual
strength load com-
parison

MAXRES residual strength increments
are performed.

- Notes:
- A. If IRST = 1 or, = 4 solution will proceed until MAXRES fatigue increments have been run. Data corresponding to the last fatigue increment is saved on Tape 30 for restarting in a later run.
 - B. If IRST = 2 or, = 4 solution begins at the fatigue increment following that in Note A. MAXFAT must be increased to include both the increments run in A., plus those in the new run.
 - C. For restarting, all data must be input, as when not restarting, and the proper Tape 30 must be provided.
 - D. If LOVRD.NE.0, the residual strength calculation continues until MAXRES steps have been performed. If LOVRD.EQ.0, the residual strength calculation ceases when the least failure load decreases from one residual strength increment to the next.
 - E. If MODEX.NE.0, all data is read into the program, and core required for the model is determined.
 - F. MAXFAT and MAXRES load steps are performed if no residual strength failure or fatigue failure occurs.

<u>Column</u>		<u>Content</u>
16-25	COPROP (N,2)	= 0.0
26-35	COPROP (N,3)	= 0.0
36-45	COPROP (N,4)	= 1.0
46-55	COPROP (N,5)	= Reduced flexural inertia
56-65	COPROP (N,6)	= Reduced flexural inertia

Notes: A. Reduced flexural inertia $I = \frac{AGL^2}{12E}$

where E = Modulus of elasticity

A = Axial area

G = Shear modulus

L = Ply Thickness

Cards 7, 8, 9

3 Blank Cards

Card 10 Beam Data 7I5

<u>Column</u>		<u>Content</u>
1-5	NEL	Element number
6-10	NI	Node I
11-15	NJ	Node J
16-20	NK	Node K
21-25	MAT	Material number
26-30	MEL	Geometric property number

Notes: A. Nodes I, J, and K are described in Figure A-A.

B. Card 10 is repeated NPAR(2) times

C. Membranes

Card 1 Control Information 7I5

<u>Column</u>		<u>Content</u>
1-5	NPAR(1)	= 4
6-10	NPAR(2)	Number of elements

Card 3 Ultimate Static Strengths 3F1D.0

<u>Columns</u>		<u>Contents</u>
1-10	FTU(I,1)	Interlaminar normal tensile strength
11-20	FTU(I,2)	Interlaminar normal compressive strength
21-30	FTU(I,3)	Interlaminar shear strength

Card 4 Number of residual strength curves 3I5

<u>Columns</u>		<u>Contents</u>
1-5	NCB(I,1)	Number of interlaminar normal tensile strength curves
6-10	NCB(I,2)	Number of interlaminar normal compressive curves
11-15	NCB(I,3)	Number of interlaminar shear strength curves

Card 5 Residual Strength Curve Parameters 3F10.0

<u>Column</u>		<u>Contents</u>
1-10	STRP(3(I-1)+1, N, K)	σ/σ_u
11-20	STRP(3(I-1)+2, N, K)	Tangency point A
21-30	STRP(3(I-1)+3, N,K)	Coefficient B

- Notes:
- A. Card 5 is repeated NCB(I,K) times (N=1, NCB (I,K))
 - B. This series of cards is then repeated 3 times K = 1,3 for normal compression, and shear.
 - C. Finally the sequence of Cards 3-5 is repeated NPAR(5) times (I = 1, NPAR (5)). For any component, curves must be input in order of increasing σ/σ_u .

Card 6 Geometric Property Cards 15,6F10.0

<u>Column</u>		<u>Content</u>
1-5	N	Geometric property number
6-15	COPROP(N,1)	Axial Area

<u>Columns</u>		<u>Content</u>
26-30	ID(N,5)	= 1
31-35	ID(N,6)	= 1
36-45	X(N)	X - Ordinate
46-55	Y(N)	Y - Ordinate
56-65	Z(N)	Z - Ordinate

- Notes:
- A. Model must be oriented in Y-Z Plane.
 - B. Boundary condition code = 0 for force B.C.
= 1 for zero displacement B.C.
 - C. Model should be oriented with the Y-Axis coinciding with the laminate 0° axis

B. Beams

<u>Card 1</u>	<u>Control Data</u>	<u>6I5</u>
<u>Columns</u>		<u>Contents</u>
1-5	NPAR(1)	= 2
6-10	NPAR(2)	Number of beam elements
11-15	NPAR(3)	Number of geometric property cards
16-20	NPAR(4)	= 0
21-25	NPAR(5)	Number of material property cards
26-30	NPAR(6)	Maximum number of curves representing the residual strength of any component of any material

<u>Card 2</u>	<u>Material Property Card</u>	<u>I5, 2F10.0</u>
<u>Column</u>		<u>Contents</u>
1-5	N Material number	
6-15	E(N)	Modulus of Elasticity
16-25	G(N)	Poisson's ratio

- Note:
- A. Card 2 is repeated NPAR(5) times

<u>Columns</u>		<u>Content</u>
11-20	TOLER	Multiple element failure tolerance
21-30	REDMOD	Failed element reduced modulus value

- Notes: A. FATLOD is the ratio of the loading applied to the finite element model with cards II-C-11, III-1, and III-3 maximum fatigue loading.
- B. TOLER is a decimal fraction indicating the range of elemental failure loads which will be considered equivalent.

Card 5 Fatigue Cycles 8F10.0

<u>Columns</u>		<u>Content</u>
1-10	CYCLEN(2)	Number of cycles for second fatigue inc.
11-20	CYCLEN(3)	Number of cycles for second fatigue inc.

Repeated (MAXFAT-1) times

- Notes: A. If MAXFAT.LT.2 skip this card
- B. First fatigue increment is always the static case i.e. CYCLEN(1) = 1.0

II GRID INPUT DATA

A. Nodes

<u>Card 1</u>	<u>Nodal Point Data</u>	<u>7I5, 3F10.0</u>
<u>Column</u>		<u>Contents</u>
1-5	N Node Number	
6-10	ID(N,1)	= 1
11-15	ID(N,2)	Y-Translation boundary condition code
16-20	ID(N,3)	Z-Translation boundary condition code
21-25	ID(N,4)	= 1

Card 3Print Indicators8I5ColumnsContents

1-5	KEY(1)	Print indicator for grid
6-10	KEY(2)	Print indicator for loads
11-15	KEY(3)	Print indicator for beam forces
16-20	KEY(4)	Print indicator for beam stresses
21-25	KEY(5)	Print indicator for membrane stresses (Y-Z)
26-30	KEY(6)	Print indicator for membrane stresses (1-2)
31-35	KEY(7)	Print indicator for elemental failure load ratios
36-40	KEY(8)	Print indicator for displacements

- Notes:
- A. Forces, Stresses, and displacements correspond to the loading applied to model in cards II-C-11, III-1 and III-3.
 - B. Elemental failure load ratios are the ratios of the load required to fail a particular element to the load which is applied to the model.
 - C. Stresses and displacement are output in the coordinate systems defined in Figure A-3.
 - D. KEY(I) = 0, Quantities are not printed
KEY(I) = 1, Quantities are printed
 - E. For KEY(4) and KEY(6)
KEY(I) = 1, Print at fatigue failure only
 = 2, Print at residual strength failures only
 = 3, Print at each increment.

Card 4Fatigue Parameters3F10.0ColumnsContent

1-10	FATLOD	Ratio of applied load to fatigue load
------	--------	---------------------------------------

<u>Column</u>	<u>Content</u>
11-15	NPAR(3) Number of materials
16-20	NPAR(4) = 1
21-25	NPAR(5) = 2
26-30	NPAR(6) = 1
31-35	NPAR(7) Maximum number of curves representing the residual strength of any component of any material

Card 2 Material Property Information 2I5,20X,F10.0

<u>Column</u>	<u>Content</u>
1-5	I Material identification number
6-10	NTC(I) = 1
11-20	Blank
21-30	Blank
31-40	WANG(I) Angle of ply orientation measured counter-clockwise from the Y-Axis

Card 3 Elastic Properties 10X,4F10.0

<u>Column</u>	<u>Content</u>
1-10	Blank
11-20	E(1,2,I) E_{11}
21-30	E(1,3,I) E_{22}
31-40	E(1,4,I) ν_{12}
41-50	E(1,5,I) G_{12}

Notes: A. ν_{12} is defined such that

$$\frac{\nu_{12}}{E_{11}} = \frac{\nu_{21}}{E_{22}}$$

B. Cards 2 and 3 are repeated NPAR(3) times I = 1,NPAR(3)

Card 4 Ultimate Static Strengths 5F10.0

<u>Column</u>	<u>Content</u>
1-10	FTU(I,1) Longitudinal tensile strength

<u>Column</u>		<u>Content</u>
11-20	FTU(I, 2)	Longitudinal compressive strength
21-30	FTU(I, 3)	Transverse tensile strength
31-40	FTU(I, 4)	Transverse compressive strength
41-50	FTU(I, 5)	Inplane shear strength

Card 5 Number of Residual Strength Curves 5I5

<u>Column</u>		<u>Content</u>
1-5	NCM(I, 1)	Number of longitudinal tension curves
6-10	NCM(I, 2)	Number of longitudinal compression curves
11-15	NCM(I, 3)	Number of transverse tension curves
16-20	NCM(I, 4)	Number of transverse compression curves
21-25	NCM(I, 5)	Number of inplane shear curves

Card 6 Residual Strength Curve Parameters 3F10.0

<u>Column</u>		<u>Content</u>
1-10	STRP(3(I-1)+1, N, K)	σ/σ_u
11-20	STRP(3(I-1)+2, N, K)	Tangency Point A
21-30	STRP(3(I-1)+3, N, K)	Coefficient B

- Notes:
- A. Card 6 is repeated NCM(I,K) times (N=1, NCM(I,K)).
 - B. This series of cards is repeated 5 times (K=1,5) for longitudinal tension, longitudinal compression, transverse tension, transverse compression and inplane shear.
 - C. Finally, the sequence of cards, 4-6 is repeated NPAR (3) times.

Card 7 Load Multiplier 10X,F10.0

1-10	Blank	
11-20	EMUL(2, 1)	Multiplier for pressure load defined on following element cards

Cards 8, 9 and 10

3 Blank Cards

Card 11 Membrane Element Cards 6I5,2F10.0,2I5,F10.0

<u>Column</u>		<u>Content</u>
1-5	M	Element number
6-10	IE(1)	Node I
11-15	IE(2)	Node J
16-20	IE(3)	Node K
21-25	IE(4)	Node L
26-30	IE(5)	Material number
31-40	Blank	
41-50	PRESS	Pressure on I-J face
51-55	Blank	
56-60	Blank	
61-70	THICK	Ply thickness

Card 11 is repeated NPAR(2) times

Note: A. See Figure A-2 for element orientation.

III LOADS

Card 1 Nodal Forces 2I5,3F10.0

<u>Column</u>		<u>Content</u>
1-5	N	Node number
6-10	L	= 1
11-20	R(1)	= 0.0
21-30	R(2)	= Y - direction force
31-40	R(3)	= Z - direction force

Notes: A. Card 1 is repeated until all nodal forces are input.
A blank card ends forc input.

Card 2 Nodal Displacement Information I5

<u>Column</u>		<u>Content</u>
1-5	NDISPS	Number of prescribed displacements

Card 3Nodal Displacements2I5,F10.0ColumnContent

1-5	NOD	Node number
6-10	NDIR	Direction of displacement = 2, Y; = 3, Z
11-20	VAL	Prescribed displacement value

Notes: A. Card 3 is repeated NDISPS times

Card 4Load MultiplierF10.0ColumnContent

1-10	STR(1,1)	= 1.0
------	----------	-------

General Considerations:

1. Beam and membrane group input may be interchanged.
2. Input quantity units need only be consistent.
3. Certain data input reduction schemes were incorporated in the SAPIV code. These are carried into the FLAC code also, but not described here. They are fully described in Reference 5.

APPENDIX B
MEMBRANE AND SHEAR SPRING STRESS ANALYSIS MODEL

The finite element stress analysis model selected for incorporation into the fatigue analysis methodology consists of membrane elements and beam elements constrained to act as shear springs. This particular arrangement was chosen primarily because of two considerations. First, the model of membrane elements and shear spring elements yields considerably more economical results than three-dimensional brick finite element models. Secondly, the constrained beam elements were selected so as to alleviate the tedium of developing a specialized shear spring element. Both of the element types used and the various routines needed for their development were adapted from the SAP IV analysis code (ref. 5).

The basic model of a laminated composite plate is depicted in figure B-1. Since membrane elements have no bending or out of plane stiffness, the plate modeled must be balanced and mid-plane symmetric. This removes the possibility of any material induced bending. In addition, no bending may be applied to the model through the various loadings available. Due to the restriction that the laminate be balanced and mid-plane symmetric, no shearing forces may exist there. Hence, the interface at the mid-plane need not be modeled.

In the model as described, the only degrees of freedom which are allowable are in-plane translations. Thus, all other components, three rotations and the out of plane translations, must be constrained out of the model. The constraint upon nodal rotations in the model causes the beam elements to deflect as shown in figure B-2. In order that static equilibrium be satisfied, the moment, M , caused by the shearing forces, F , is reacted by constraint forces at the nodes.

In figure B-2, the relationship between ply thickness, shear modulus and beam flexural moment of inertia is also depicted. The relation for "I" given in the figure must be used in the finite element model so the interlaminar element will have the proper force-displacement relationship. The area "A" used in the flexural

inertia computation is defined in figure B-3. The beam, connected to a node, must carry the interlaminar shear forces corresponding to some portion of the membrane elemental areas also connected to that node. In the figure there are four membranes at node in question, thus the area utilized in the flexural inertia computation corresponds to one-fourth the sum of the areas of the membranes. Using the method depicted in the figure, a consistent allocation of shear areas is obtained.

APPENDIX C
QUASI THREE-DIMENSIONAL FINITE ELEMENT ANALYSIS

To verify the membrane and shear spring analysis model, comparisons were made with a finite difference solution and with a quasi three-dimensional analysis. The quasi three-dimensional analysis was supplied by Dr. G. L. Roderick, NASA Langley. This appendix contains a brief description of the quasi three-dimensional formulation. The finite element model used in implementing the quasi three-dimensional model is also described.

The quasi three-dimensional finite element model is based upon the same elasticity formulation as the finite difference solution of reference 6. The model considers the stress and strain state in an infinite coupon to be independent of the coordinate in the infinite direction (X-direction in the following and in the comparisons in the text).

The displacement field, corresponding to these stress and strain states, for a balanced symmetric laminate are:

$$\begin{aligned}u_x &= \bar{\epsilon}_x X + U_x (y, z) \\u_y &= U_y (y, z) \\u_z &= U_z (y, z).\end{aligned}\tag{C-1}$$

These displacement fields can easily be seen to yield six strain components which are independent of X.

The finite element grid used in the comparisons is shown in figure C-1. The model has a ply aspect ratio (b/h_0) of 32. Each element in the model is an eight noded quadrilateral with three-degrees of freedom per node. The nodes are situated at the four vertexes and at the four mid-sides. The material properties used in the analysis were previously listed in table 1.

REFERENCES

1. McLaughlin, P.V., Jr., Kulkarni, S.V., Huang, S.N., and Rosen, B.W., "Fatigue of Notched Fiber Composite Laminates, Part I: Analytical Model," NASA CR-132747, March 1975.
2. Kulkarni, S.V., McLaughlin, P.V., Jr., and Pipes, R.B., "Fatigue of Notched Fiber Composite Laminates, Part II: Analytical and Experimental Evaluation," NASA CR-145039, April 1976.
3. Ramkumar, R.L., Kulkarni, S.V., and Pipes, R.B., "Evaluation and Expansion of an Analytical Model for Fatigue of Notched Composite Laminates," NASA CR-145308, March 1978.
4. Pifko, A., Armen, H., Jr., Levy, A., and Levine, H., "PLANS-- A Finite Element Program for Nonlinear Analysis of Structures, Volume II - Users Manual," NASA CR-145244, May 1977.
5. Bathe, K., Wilson, E.L., and Peterson, F.E., "SAP IV, A Structural Analysis Program for Static and Dynamic Response of Linear Systems," EERC-73-11, June 1973.
6. Pipes, R.B., and Pagano, N.J., "interlaminar Stresses in Composite Laminates Under Uniform Axial Extension," Journal of Composite Materials, October 1970.
7. Hashin, Z., "Failure Criterion for Uni-Directional Composites in Print, Journal of Applied Mechanics, 1980.
8. Harris, B., "Fatigue and Accumulation of Damage in Reinforced Plastics," Composites, Vol. 8 No. 4, October 1977, pp. 214-220.
9. Advanced Composites Design Guide, 3rd Edition, January 1973.

Table 1. Elastic Constants for Edge Effect Problems

$$E_{11} = 138 \text{ GPa}$$

$$E_{22} = 14.5 \text{ GPa}$$

$$G_{12} = 5.86 \text{ GPa}$$

$$\nu_{12} = 0.21$$

Table 2. Elastic Constants for Notched Plate Problem

$$E_{11} = 139 \text{ GPa}$$

$$E_{22} = 12.0 \text{ GPa}$$

$$G_{12} = 5.20 \text{ GPa}$$

$$\nu_{12} = 0.38$$

Table A-1. Failure Criteria

Tensile Fiber Mode

$$\sigma_{11} = \sigma_A^+$$

Compressive Fiber Mode

$$\sigma_{11} = -\sigma_A^-$$

Tensile Matrix Mode

$$\frac{1}{\sigma_T^+} \sigma_{22}^2 + \frac{1}{\tau^2} \sigma_{12}^2 = 1$$

Compressive Matrix Mode

$$\frac{1}{\sigma_T^-} \left[\left(\frac{\sigma_T^-}{2\tau} \right)^2 - 1 \right] \sigma_{22} + \frac{1}{4\tau^2} \sigma_{22}^2 + \frac{1}{\tau^2} \sigma_{12}^2 = 1$$

Tensile Interlaminar Mode

$$\frac{1}{\sigma_T^+} \sigma_{33}^2 + \frac{1}{\tau^2} (\sigma_{13}^2 + \sigma_{23}^2) = 1$$

Compressive Interlaminar Mode

$$\frac{1}{\sigma_T^-} \left[\left(\frac{\sigma_T^-}{2\tau} \right)^2 - 1 \right] \sigma_{33} + \frac{1}{4\tau^2} \sigma_{33}^2 + \frac{1}{\tau^2} (\sigma_{13}^2 + \sigma_{23}^2) = 1$$

Table A-1. Failure Criteria (Continued)

where

σ_A^+ = axial tensile strength

σ_A^- = axial compressive strength

σ_T^+ = transverse tensile strength

σ_T^- = transverse compressive strength

τ = shear strength

Table A-2. FLAC Routines

<u>Routine Name</u>	<u>Function</u>
FLAC	Main program: supervises stress and fatigue analysis: reads control data for analysis.
INPUTJ	Read nodal information including coordinates and boundary conditions.
ELTYPE	Supervises the calling of element routine groups.
BEAM	Calls beam element group and computes beam forces and computes interlaminar shear stresses.
PLANE	Call membrane element group and computes membrane stresses in both the laminate and lamina coordinates.
INL	Read nodal force and displacement boundary conditions: forms global force vector in blocks.
ADDSTF	Forms global stiffness vector in blocks: applies non-zero displacement boundary conditions.
PRINTD	Prints displacement.
STRESS	Supervises stress calculation over all element groups.
CALBAN	Computes maximum semi-bandwidth of global stiffness equations.
STRSC	Performs matrix multiplication to produce beam forces and membrane stresses (global coordinates).

<u>Routine Name</u>	<u>Function</u>
ELT2, TEAM, NEWBM	Beam element group: input geometric and material properties: form elemental stiffness and stress recovery matrices.
ELT3A4, PLNAX, ELAW, QUAD, FORMB, VECTOR, CROSS, DOT	Membrane element group: input geometric and material properties: form elemental stiffness and stress recovery matrices.
SOLEQ	Supervises the static solution: calls solution routine, displacement print routine and stress recovery routines.
SESOL	Performs the solution for the displacement vector.
ADSTF2	Add negative elemental stiffness matrices to the existing global stiffness matrix.
RESET	Saves information corresponding to a fatigue load stress distribution for use with a later fatigue cycle increment and retrieves information at the following fatigue cycle increment.
FAIL	Computes least failure loads using failure criterion.
ROTR	Rotates membrane stresses from laminate coordinates to lamina coordinates
STREN	Computes coefficients in failure criterion.
PARAM	Updates elemental strengths.
PREFAL	Updates elemental failure vector and checks if element has failed previously.
RESTRT	Saves data for solution restart and retrieves data when restarting.

Routine
Name

Function

PRINT

Prints fatigue analysis parameters.

ERROR

Terminates execution if storage is
insufficient

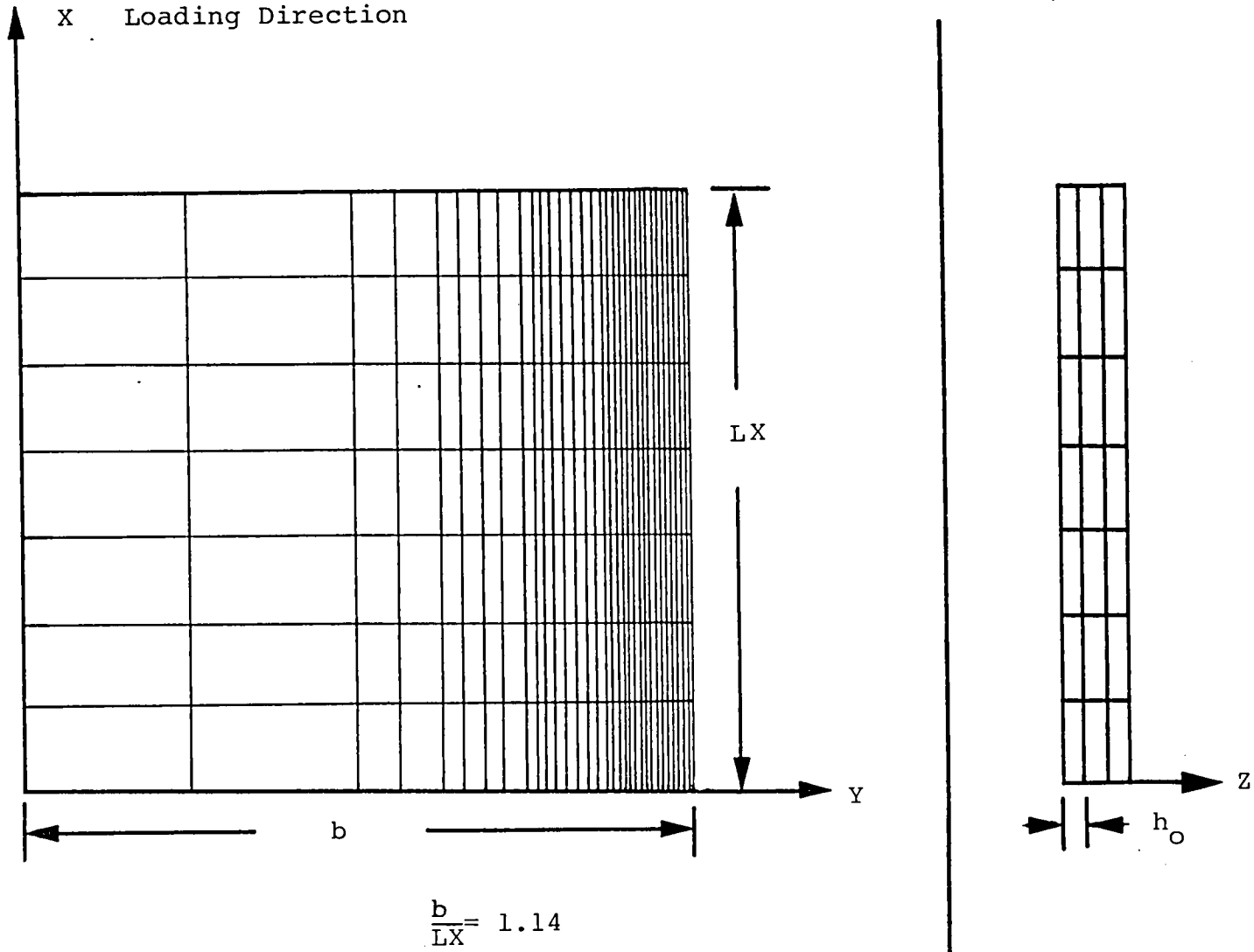


Figure 1. Edge Effect Finite Element Model

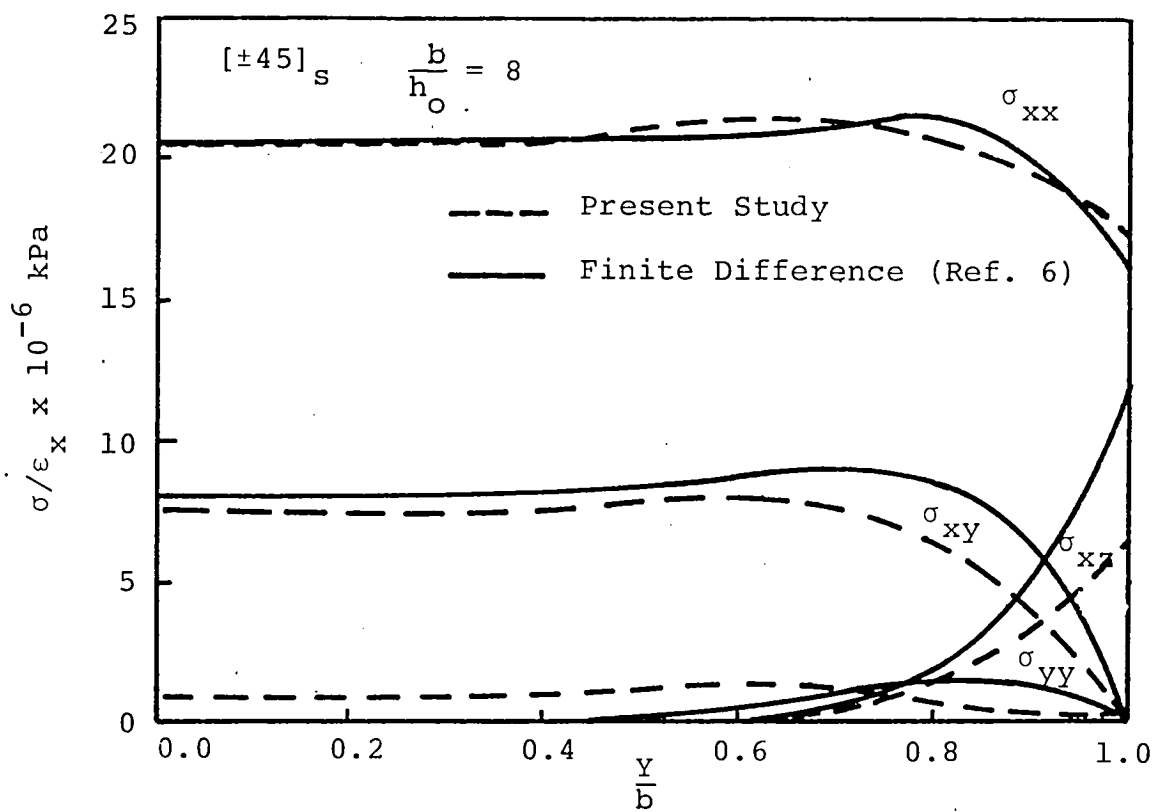


Figure 2. Comparison of Present Solution with Finite Difference Solution for $[\pm 45]_s$ Edge Effect Problem

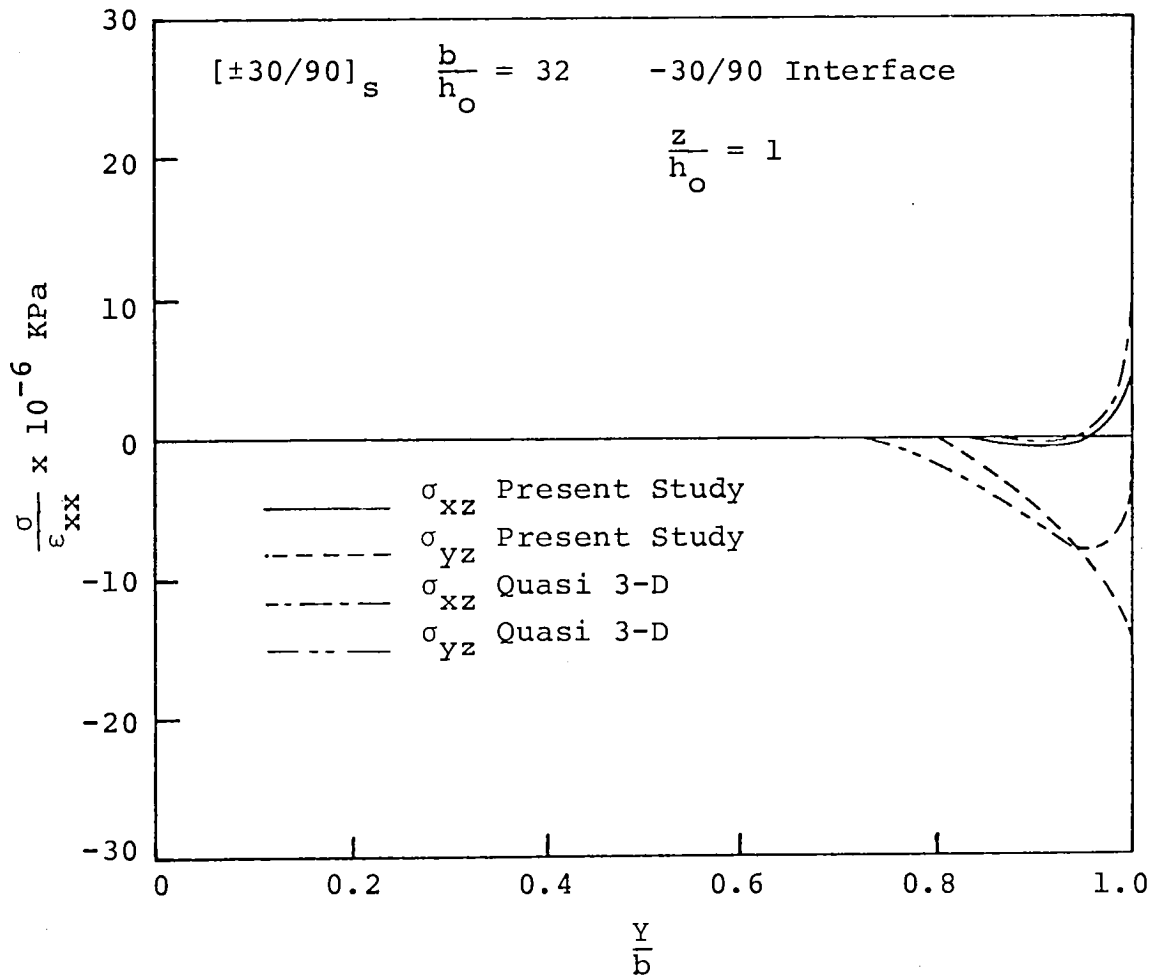


Figure 3. Comparison of Present Solution with Quasi 3-D Solution for Interlaminar Shear Stresses at $z/h_0=1$, in a $[\pm 30/90]_s$ Edge Effect Problem

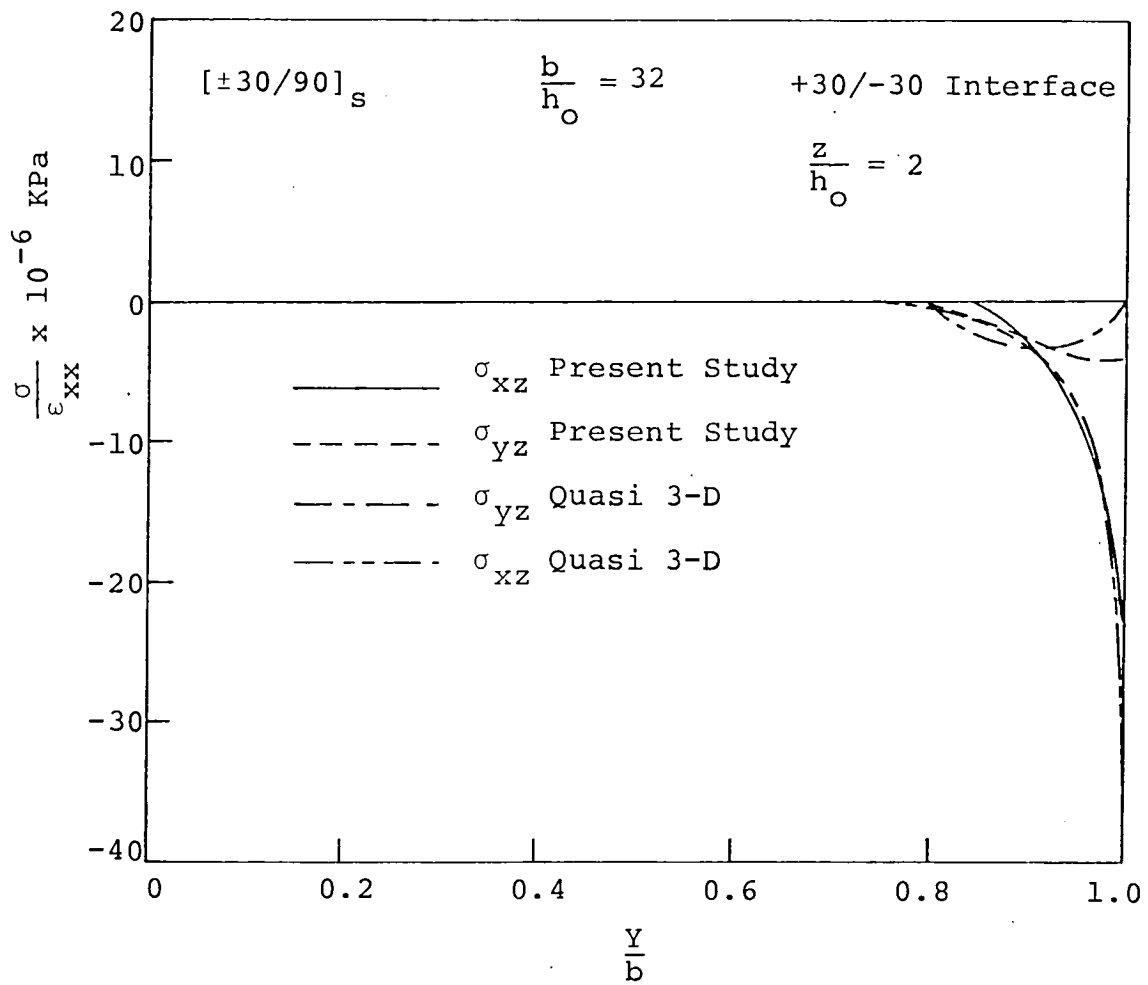


Figure 4. Comparison of Present Solution with Quasi 3-D Solution for Interlaminar Shear Stresses at $z/h_0=2$, in a $[\pm 30/90]_s$ Edge Effect Problem

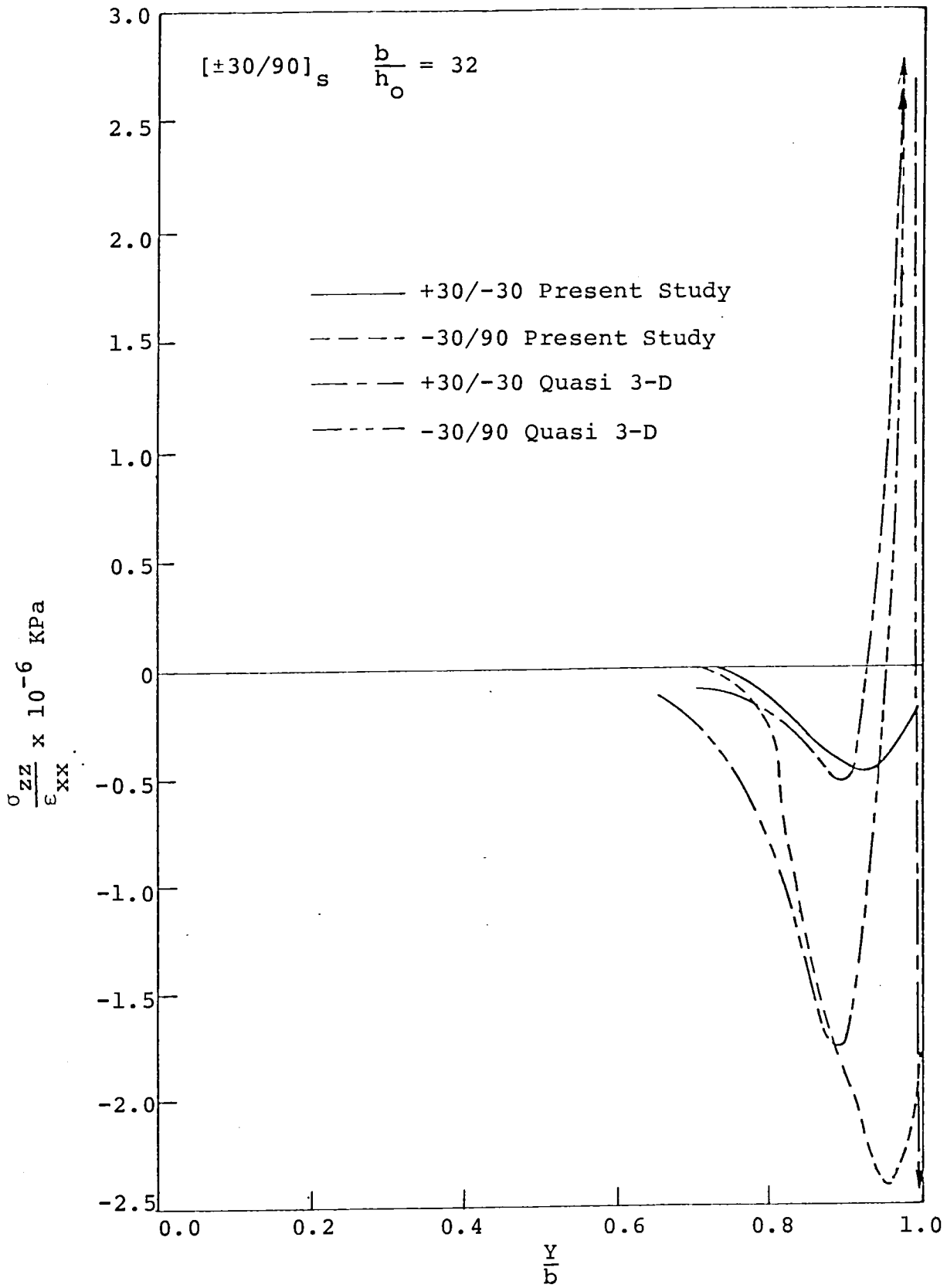


Figure 5. Comparison of Present Solution with Quasi 3-D Solution for Interlaminar Normal Stresses in a $[\pm 30/90]_s$ Edge Effect Problem

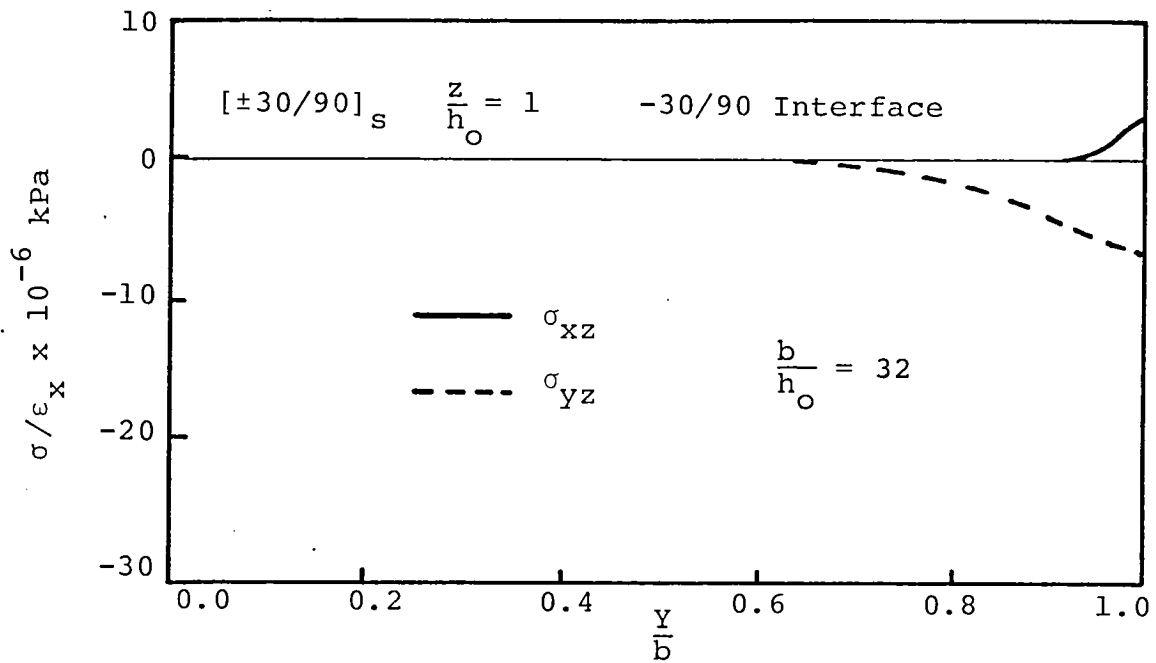


Figure 6. Interlaminar Shear Stresses Predicted by the Present Analysis at $z/h_0=1$ with Beam Stiffness Divided by Four $[\pm 30/90]_s$ Edge Effect Problem

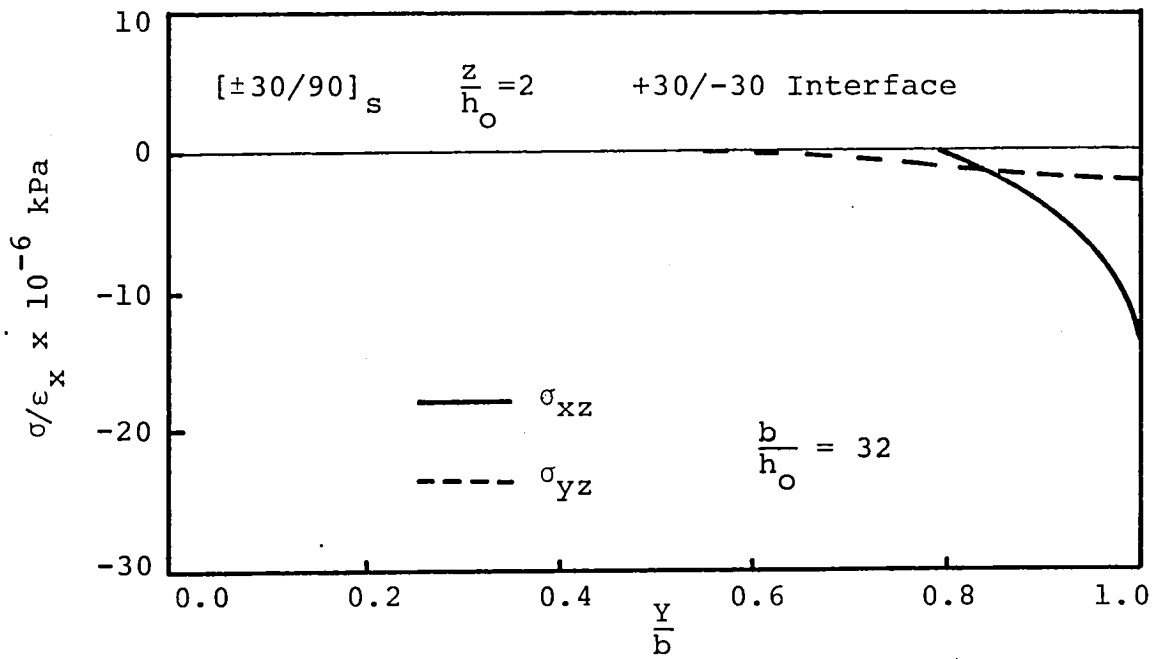


Figure 7. Interlaminar Shear Stresses Predicted by the Present Analysis at $z/h_0=2$ with Beam Stiffness Divided by Four $[\pm 30/90]_s$ Edge Effect Problem

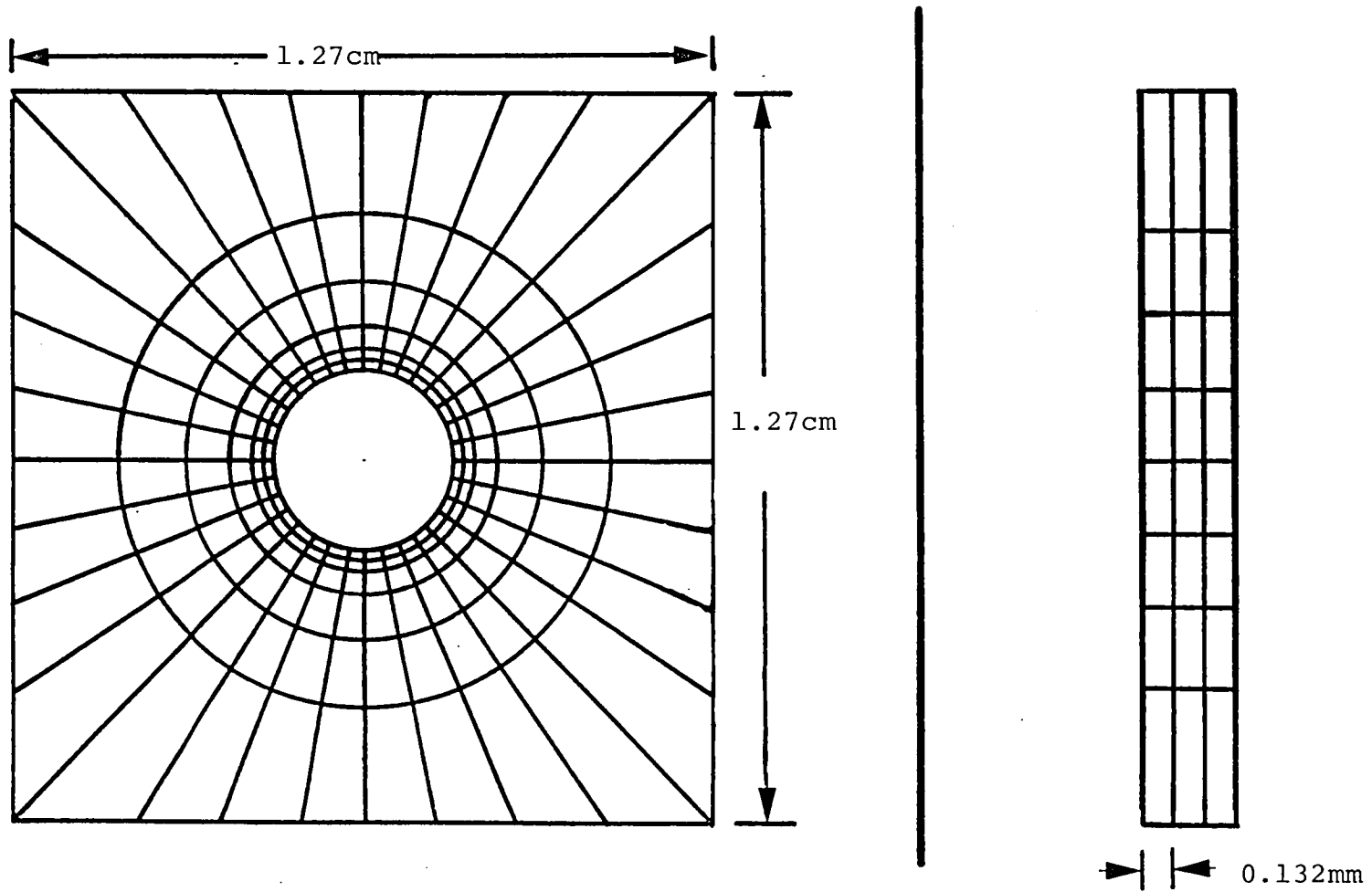


Figure 8. Notched Laminate Finite Element Model

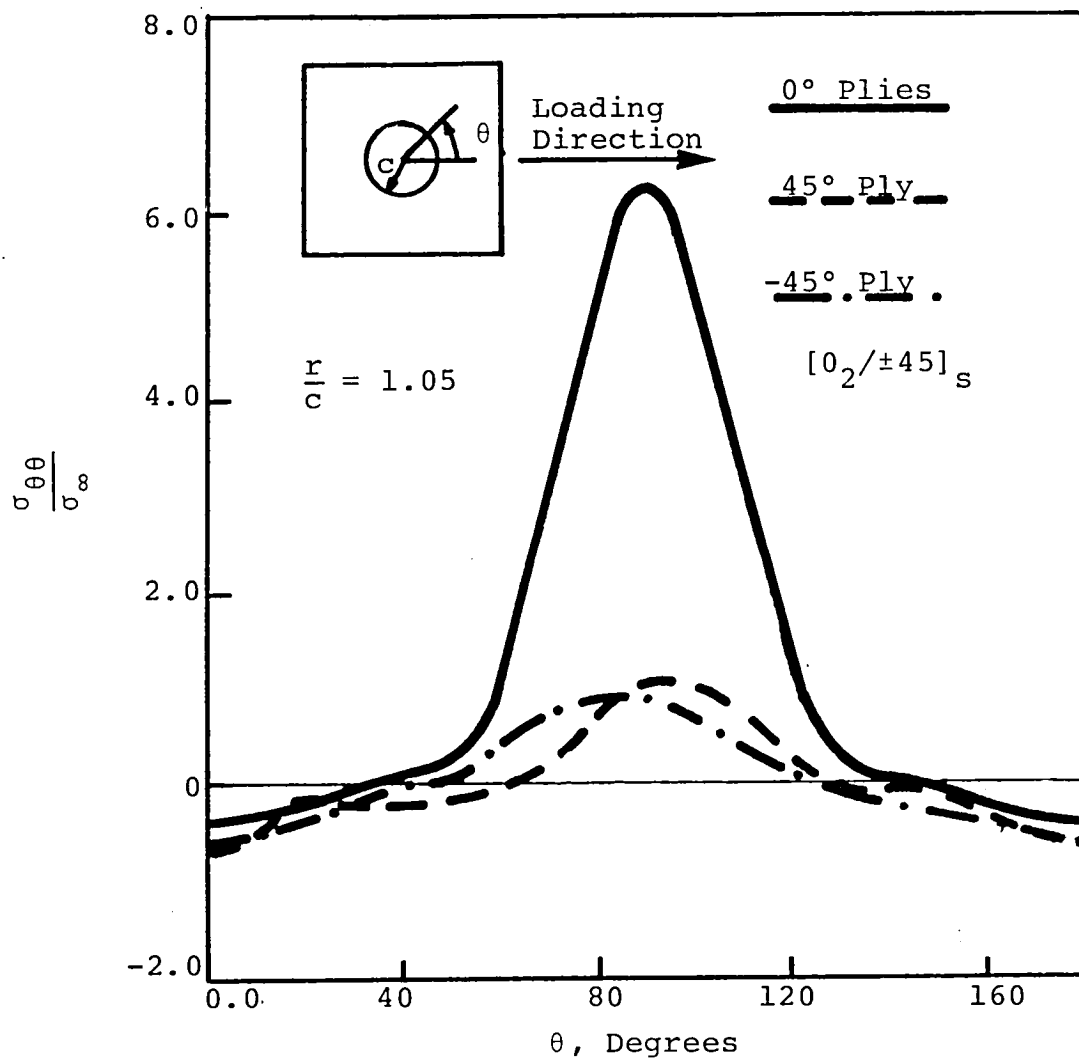


Figure 9. Circumferential Stress Near the Notch in a $[0_2/\pm 45]_s$ Notched Plate

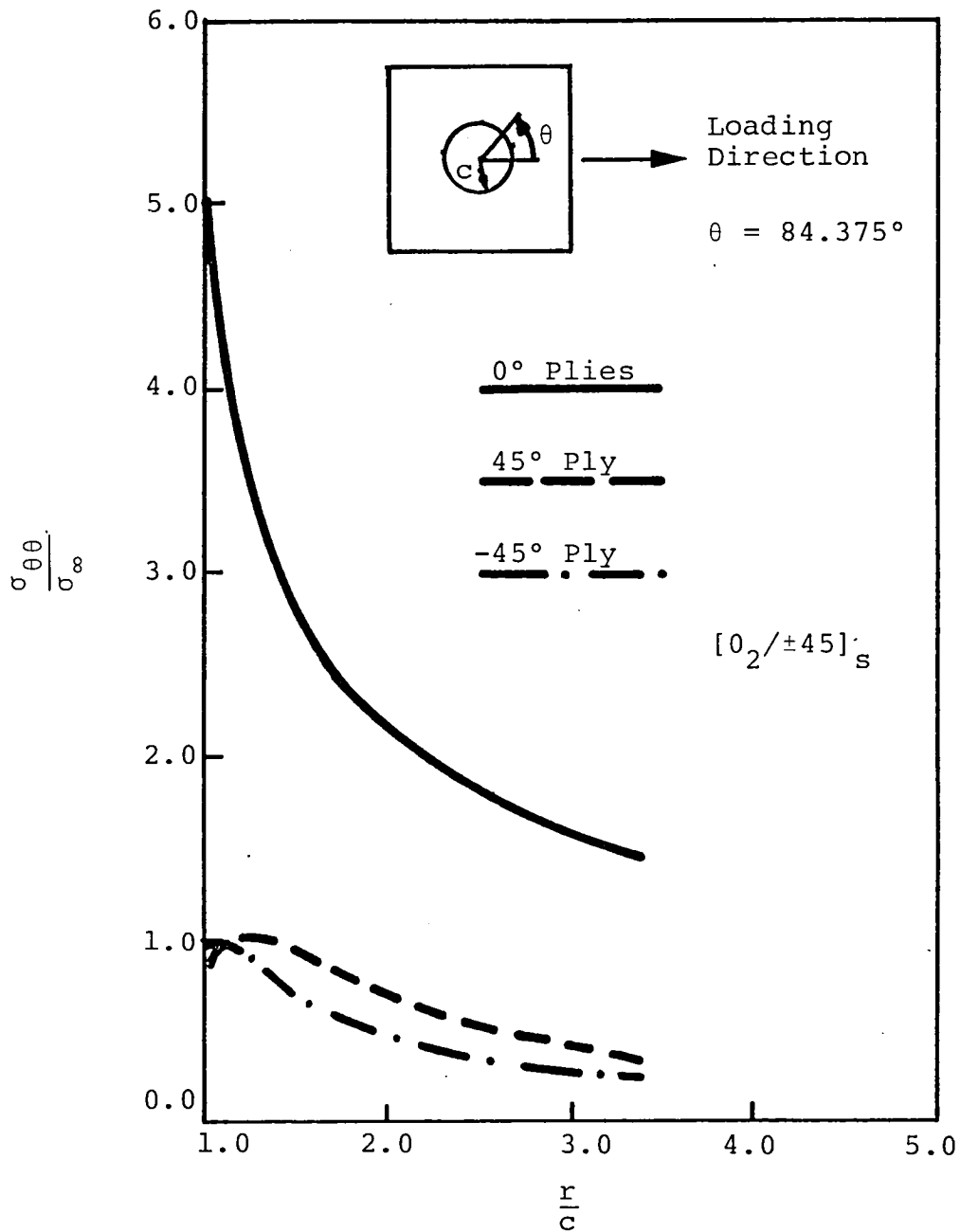


Figure 10. Circumferential Stresses at $\theta = 84.375^\circ$ in a $[0_2/\pm 45]_s$ Notched Plate

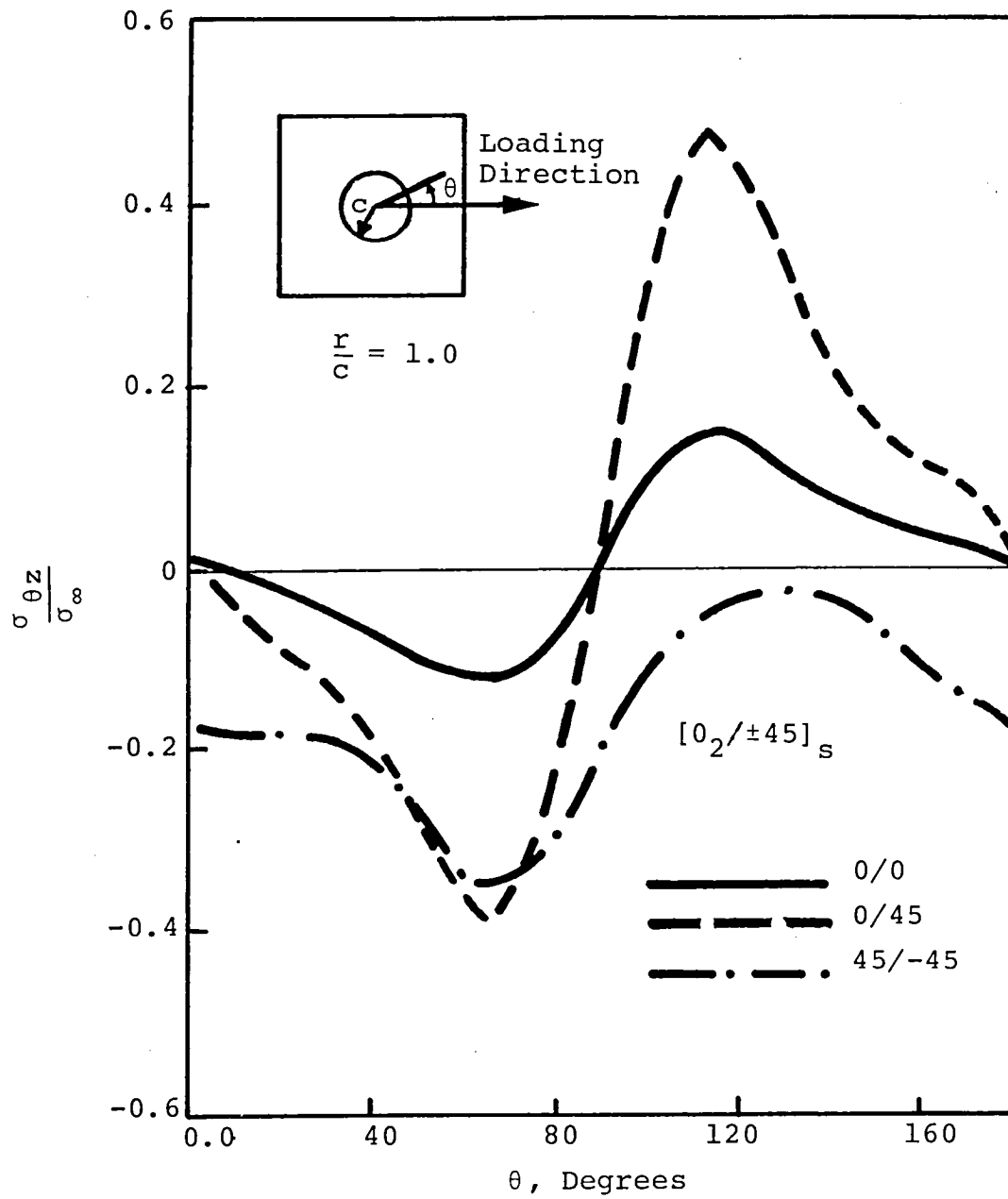


Figure 11. Interlaminar Shear Stresses at the Notch Edge in a $[0_2/\pm 45]_s$ Notched Plate

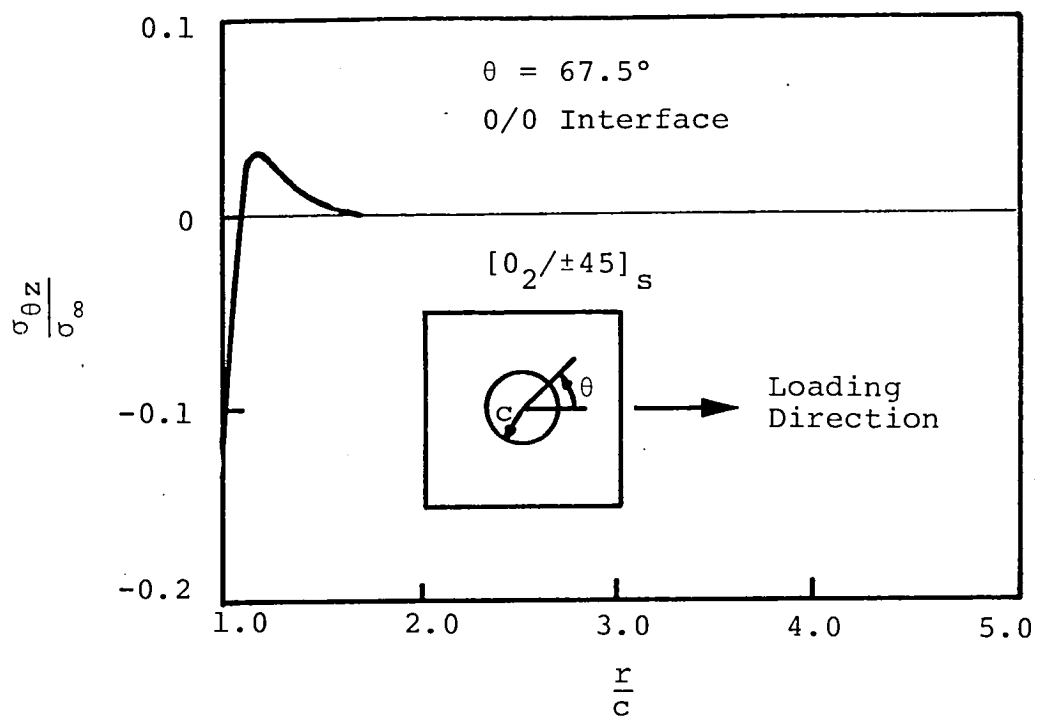


Figure 12. Interlaminar Shear Stresses at $\theta = 67.5^\circ$, 0/0 Interface, of a $[0_2/\pm 45]_S$ Notched Plate

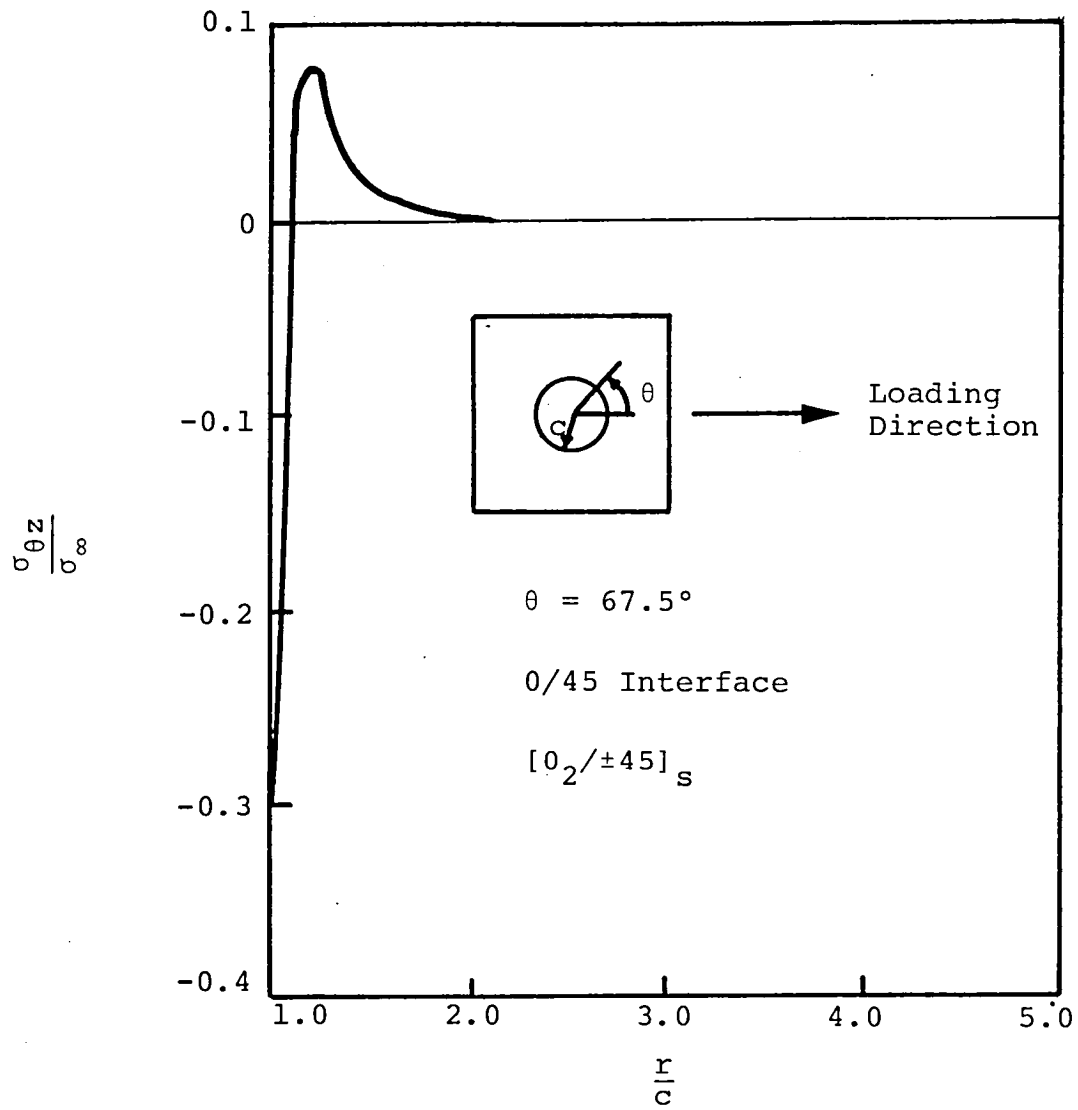


Figure 13. Interlaminar Shear Stresses at $\theta = 67.5^\circ$, 0/45 Interface, in a $[0_2/\pm 45]_S$ Notched Plate

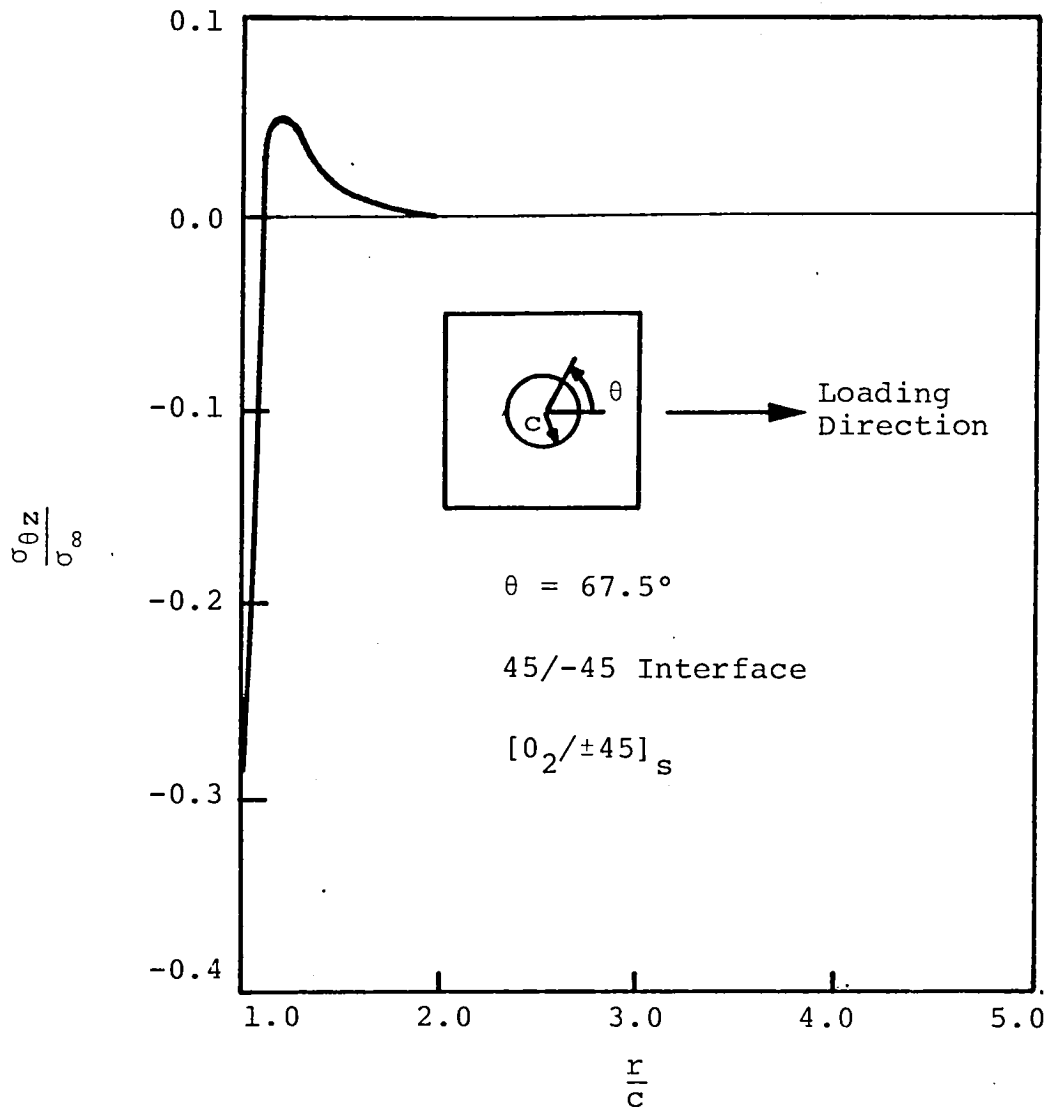


Figure 14. Interlaminar Shear Stresses at $\theta = 67.5^\circ$, 45/-45 Interface, in a $[0_2/\pm 45]_s$ Notched Plate

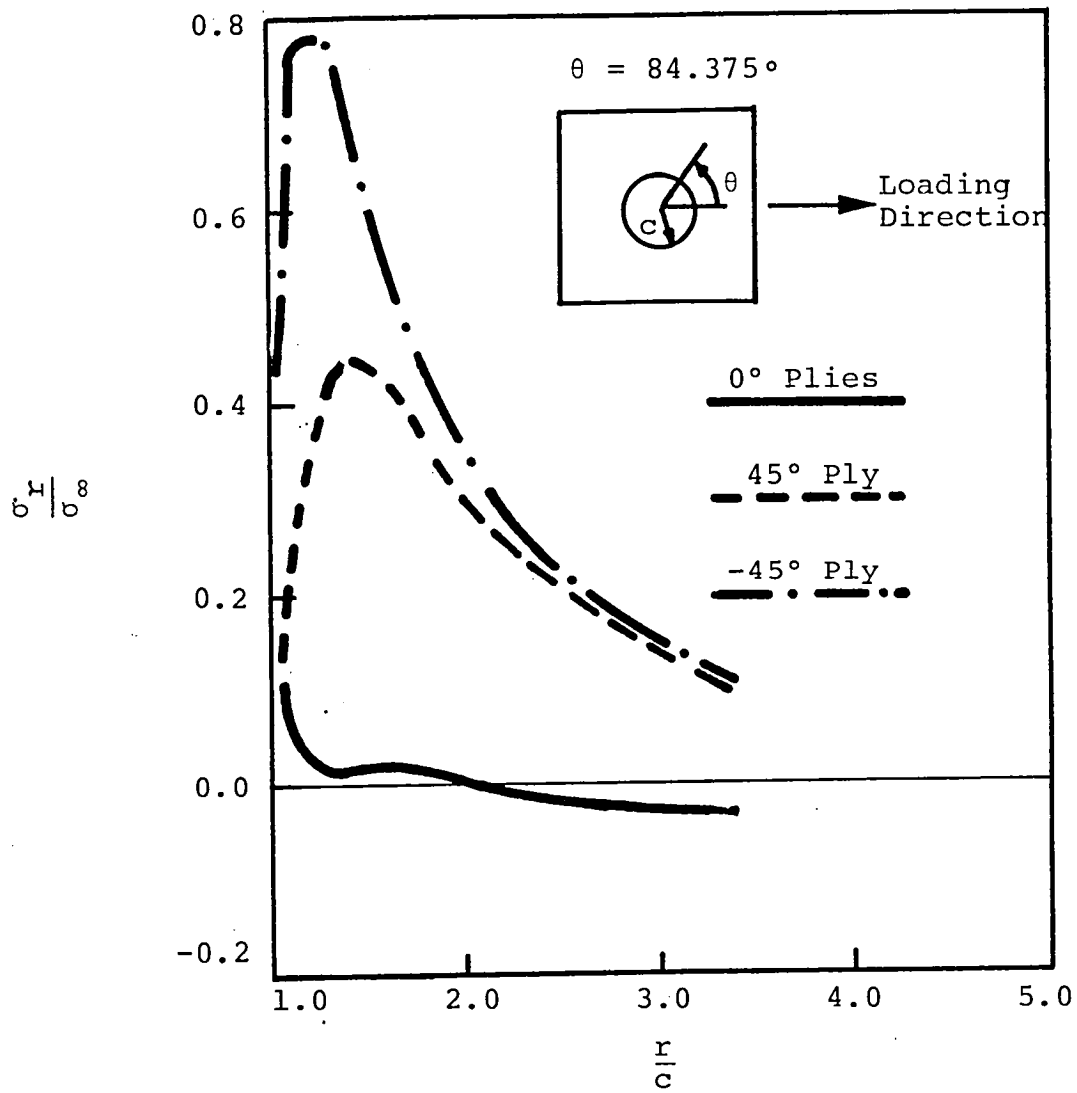


Figure 15. Radial Stresses at $\theta = 84.375$ in a $[0_2/\pm 45]_s$ Notched Plate

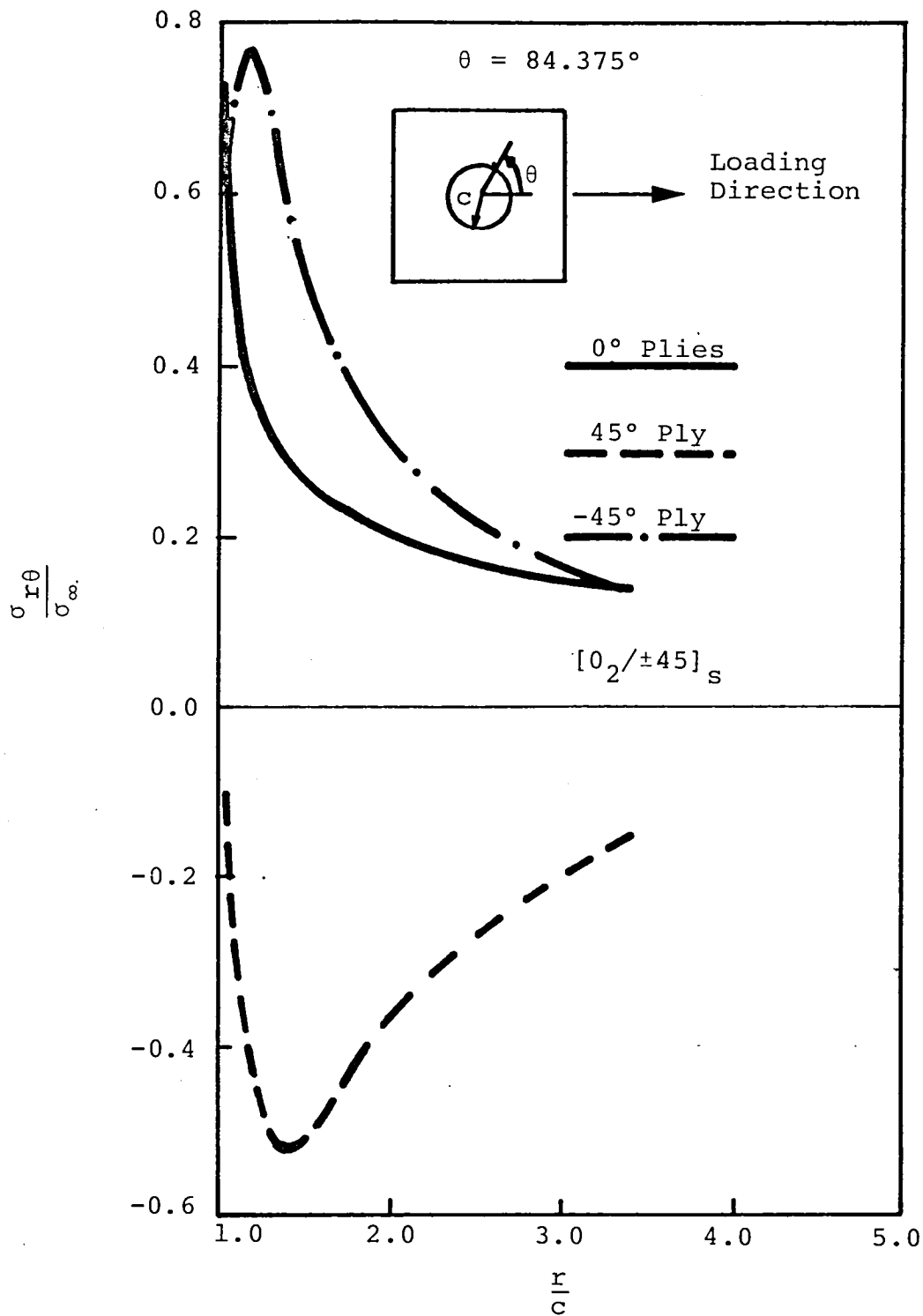


Figure 16. In-Plane Shear Stresses at $\theta = 84.375^\circ$ in a $[0_2/\pm 45]_s$ Notched Plate

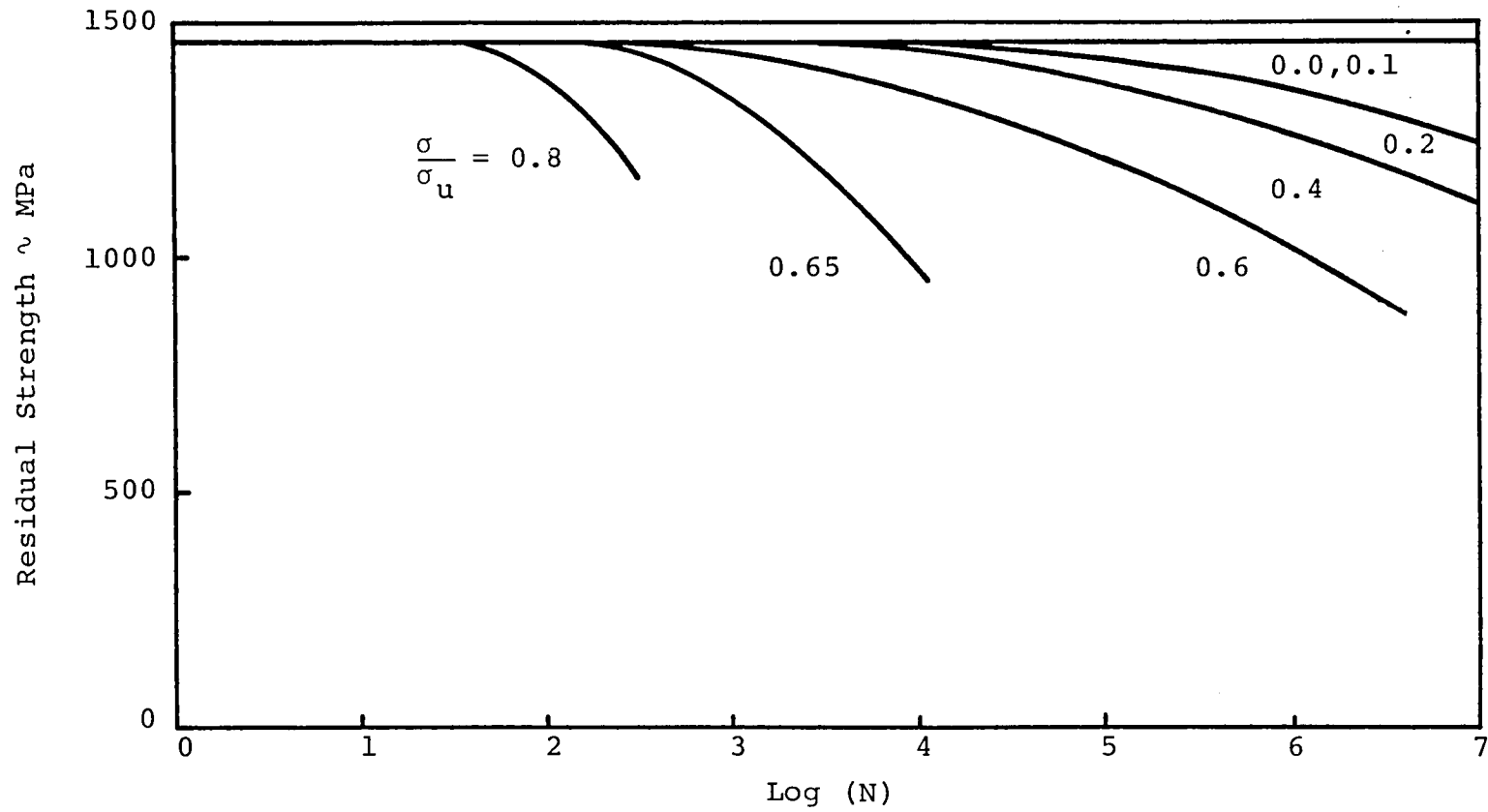


Figure 17. Lamina Residual Axial Tensile Strength

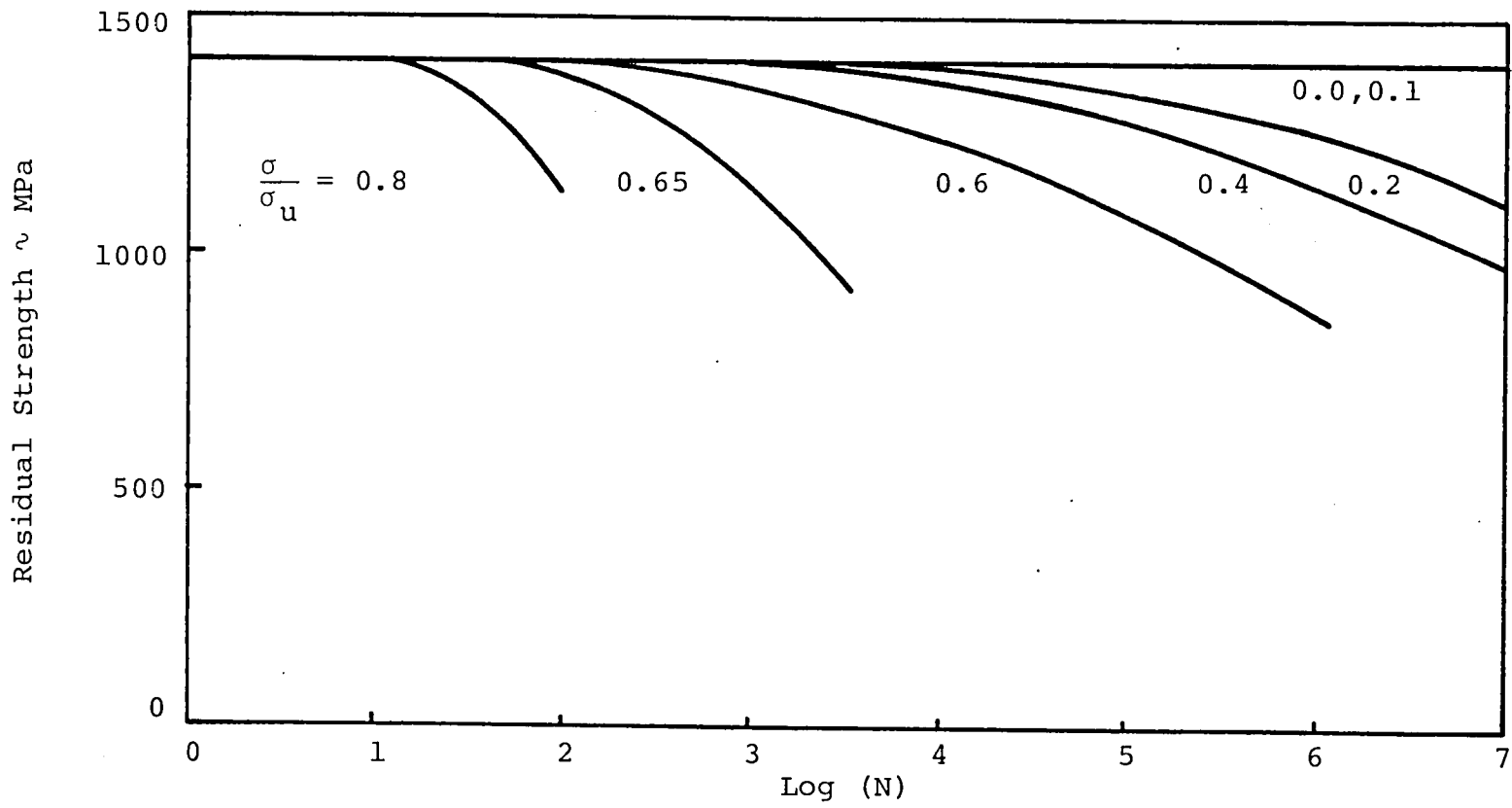


Figure 18. Lamina Residual Axial Compressive Strength

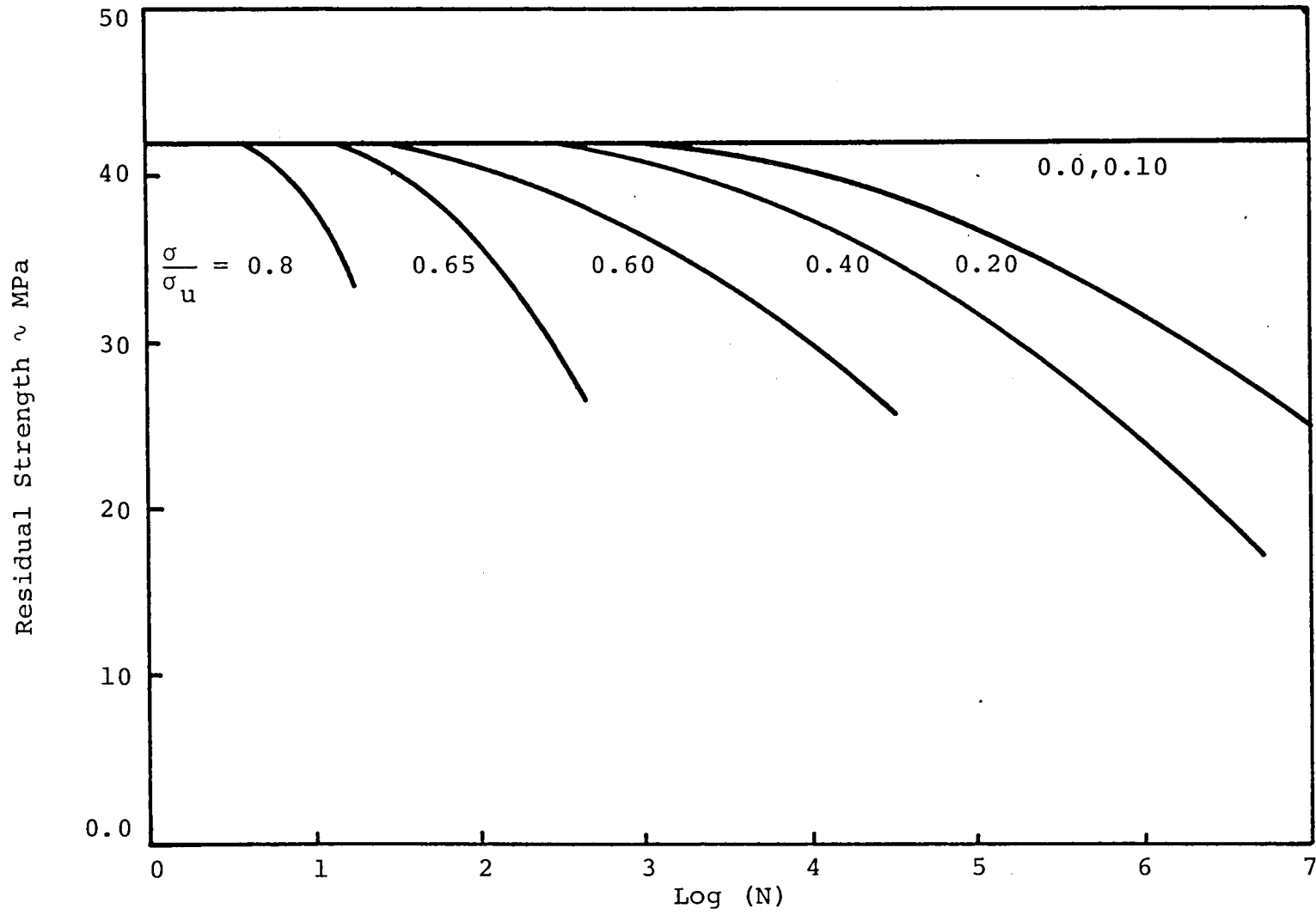


Figure 19. Lamina Residual Transverse Tensile Strength

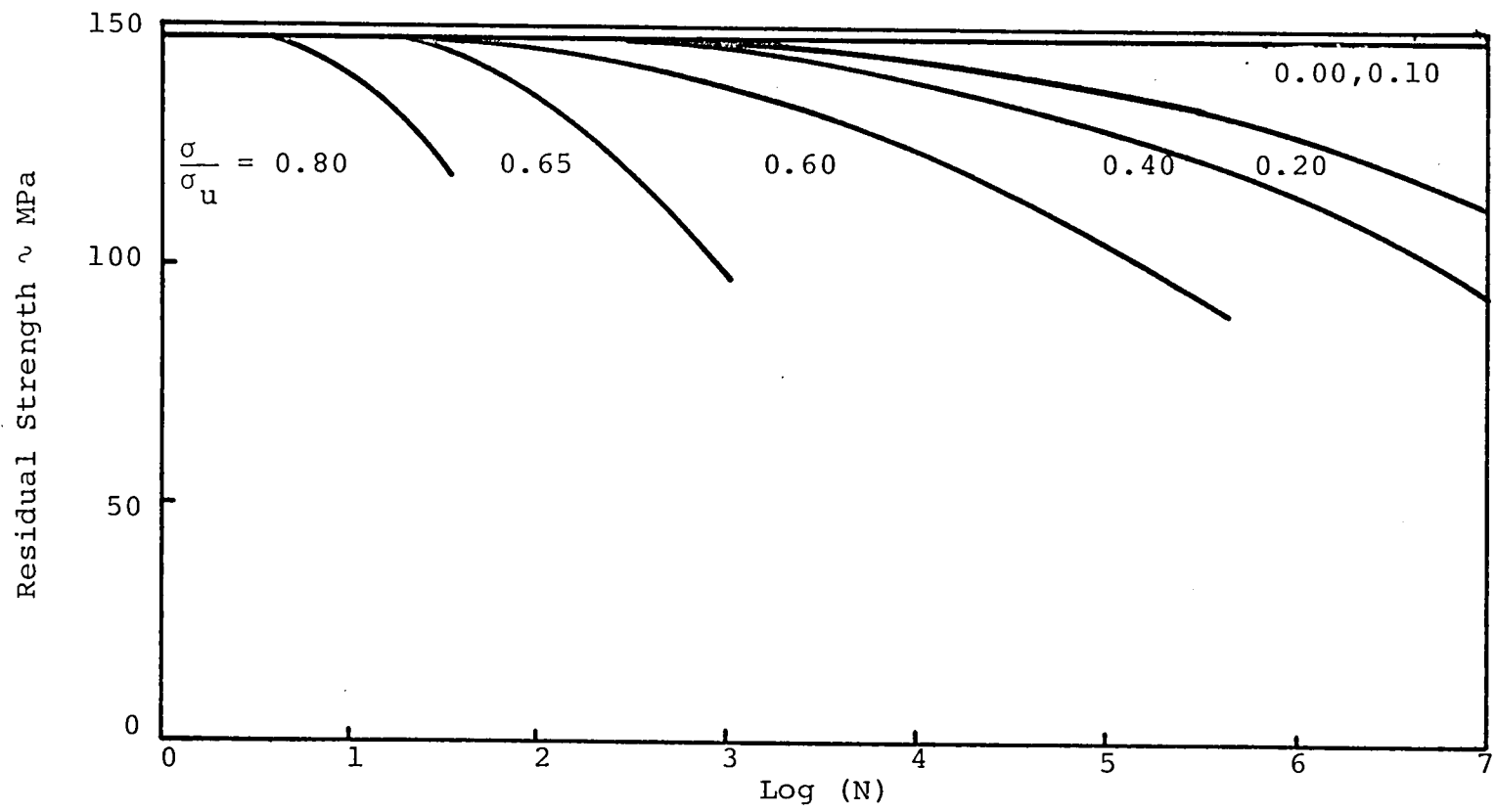


Figure 20. Lamina Residual Transverse Compressive Strength

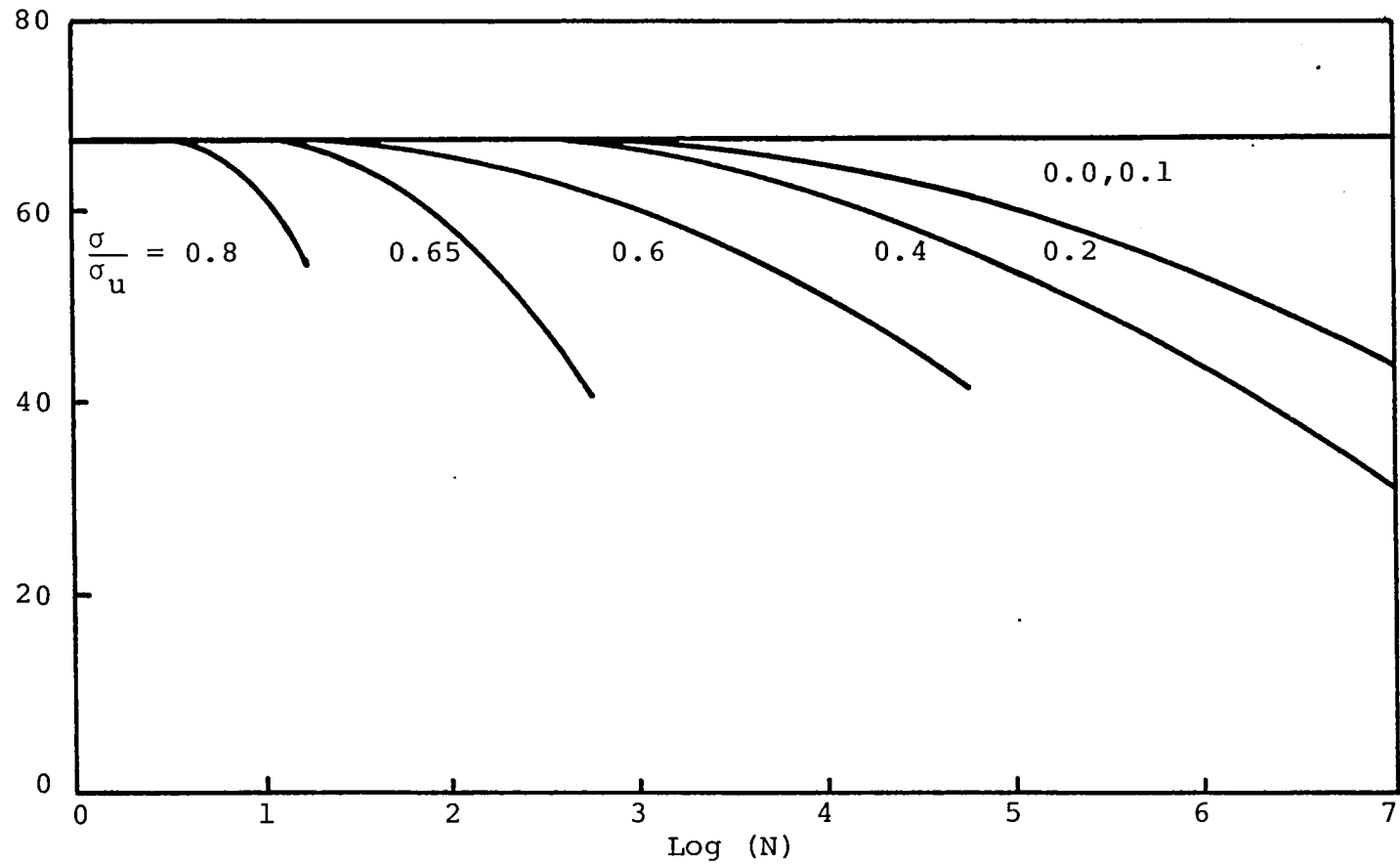
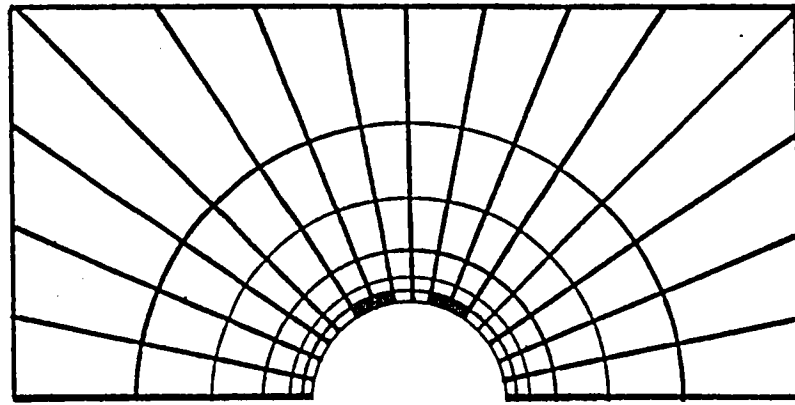
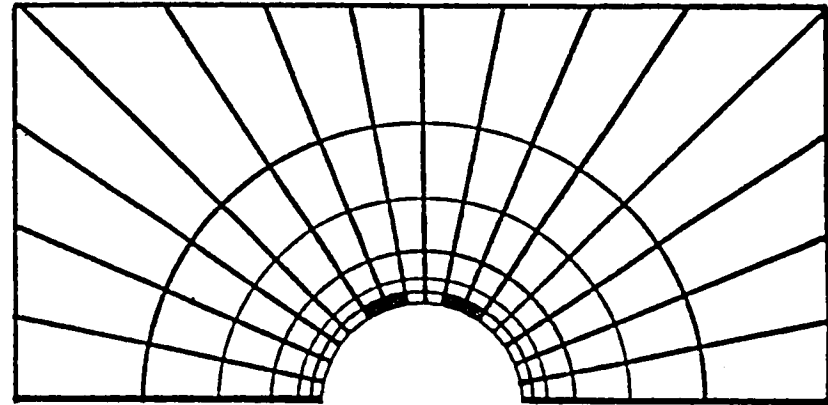


Figure 21. Lamina Residual Shear Strength

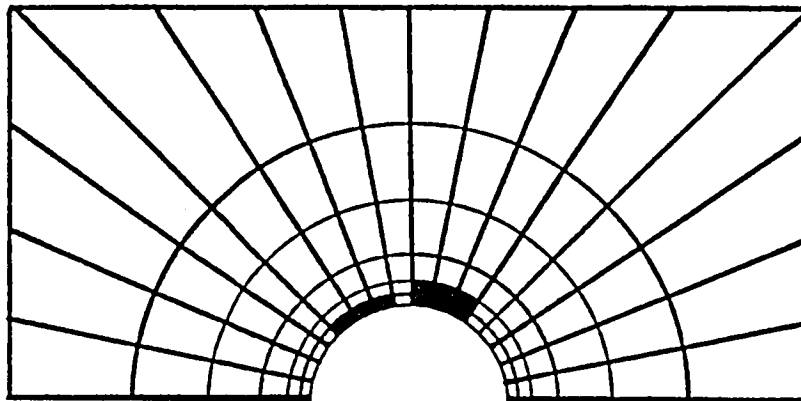


First 0° Ply

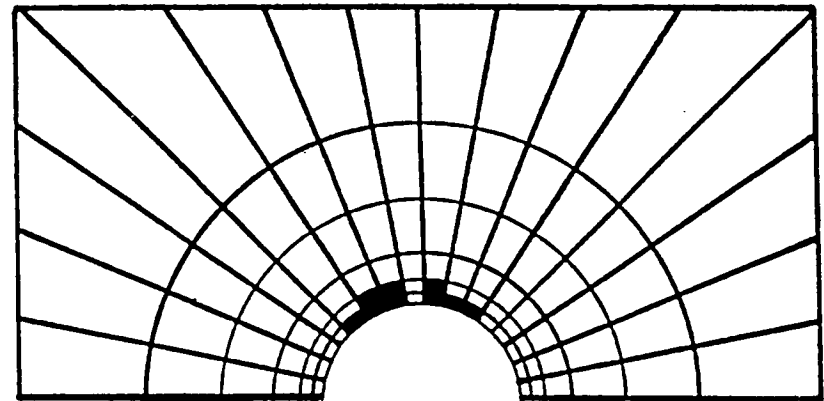


Second 0° Ply

→ Loading Direction



45° Ply



-45° Ply

Figure 22. In-Plane Damage at 179 MPa, $N = 1$, in a $[0_2/\pm 45]_S$ Notched Plate

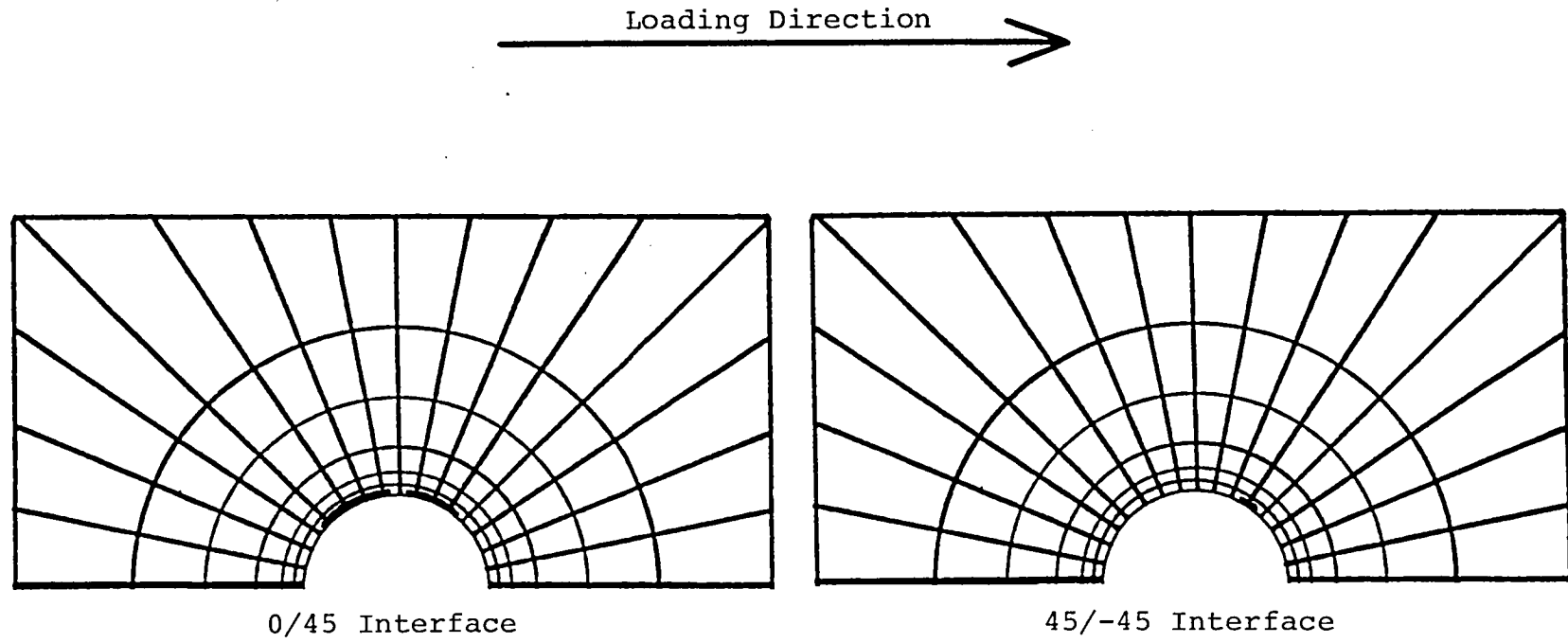


Figure 23. Interlaminar Damage at 179 MPa, $N = 1$, in a $[0_2/\pm 45]_S$ Notched Plate

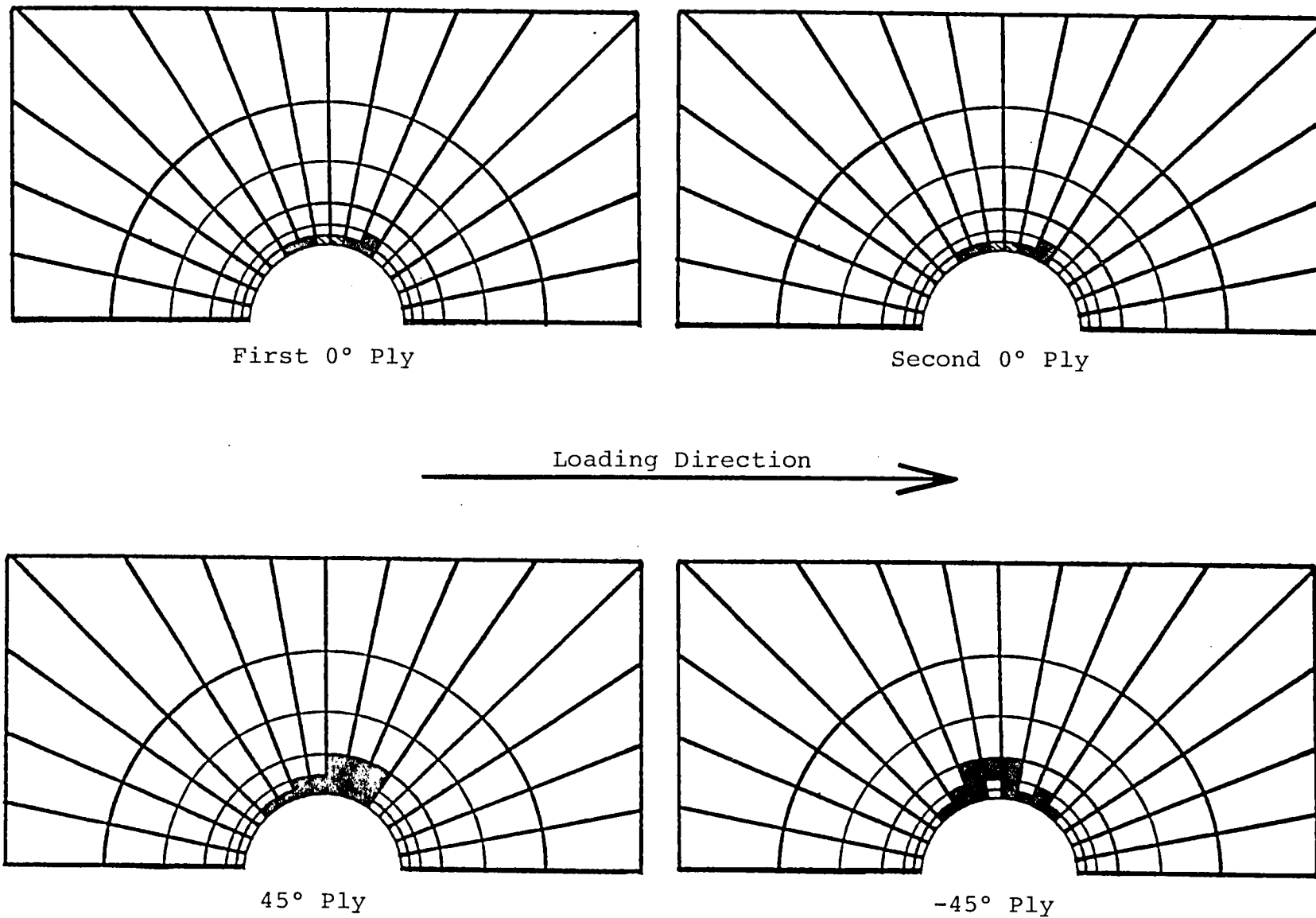


Figure 24. In-Plane Damage at 226 MPa, $N = 1$, in a $[0_2/\pm 45]_s$ Notched Plate

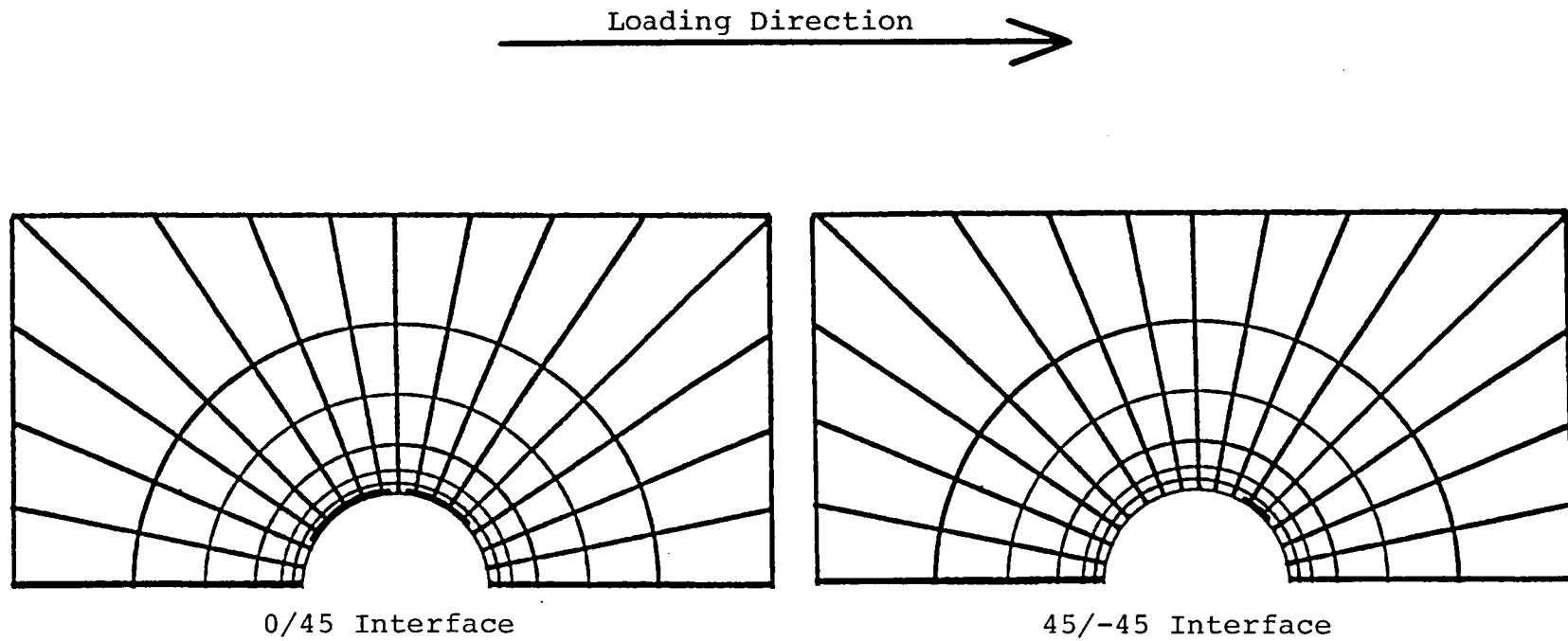


Figure 25. Interlaminar Damage at 226 MPa, $N = 1$, in a $[0_2/\pm 45]_s$ Notched Plate

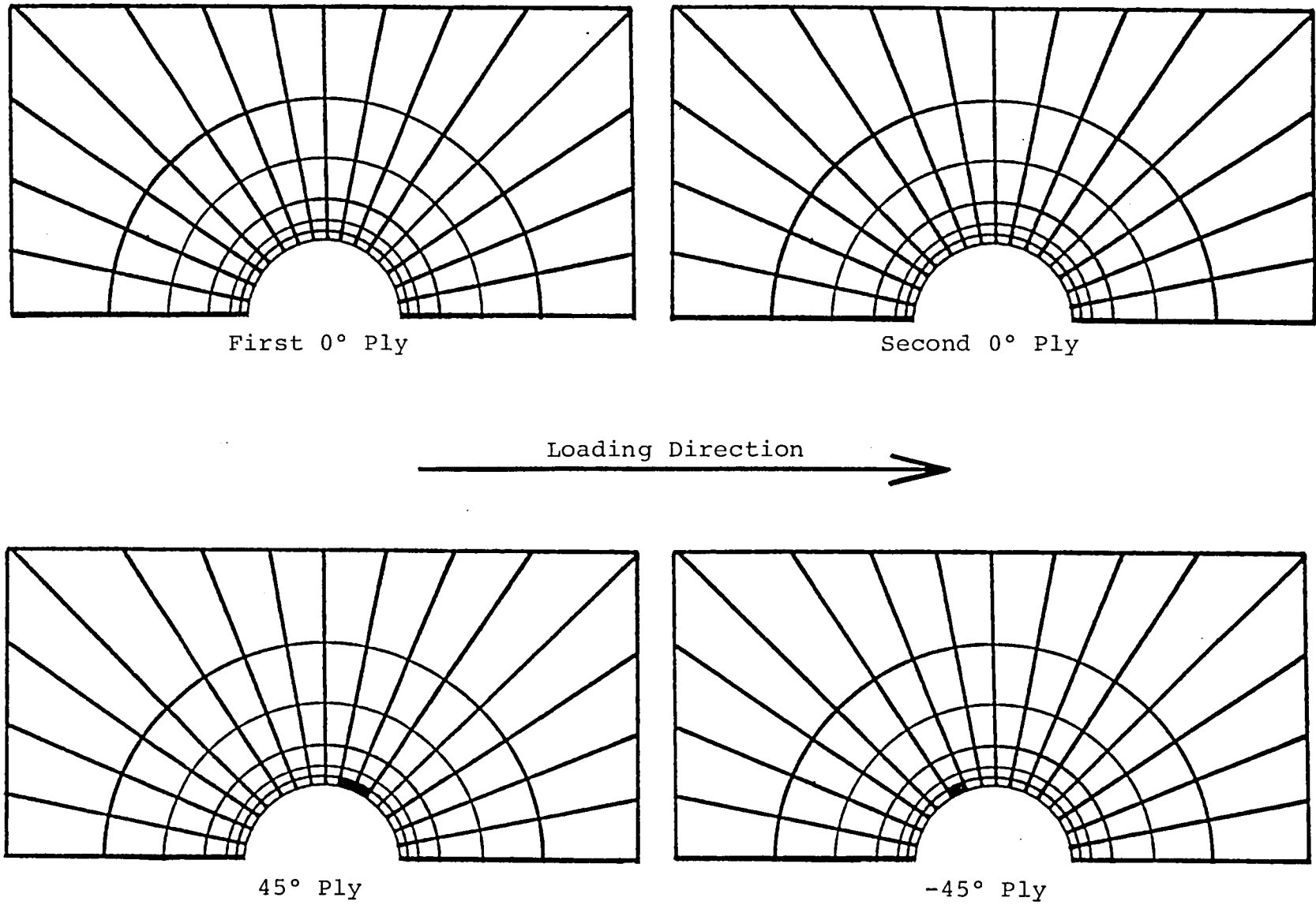


Figure 26. In-Plane Damage at Fatigue Load. 103 MPa, $N = 1000$, in a $[0_2/\pm 45]_s$ Notched Plate

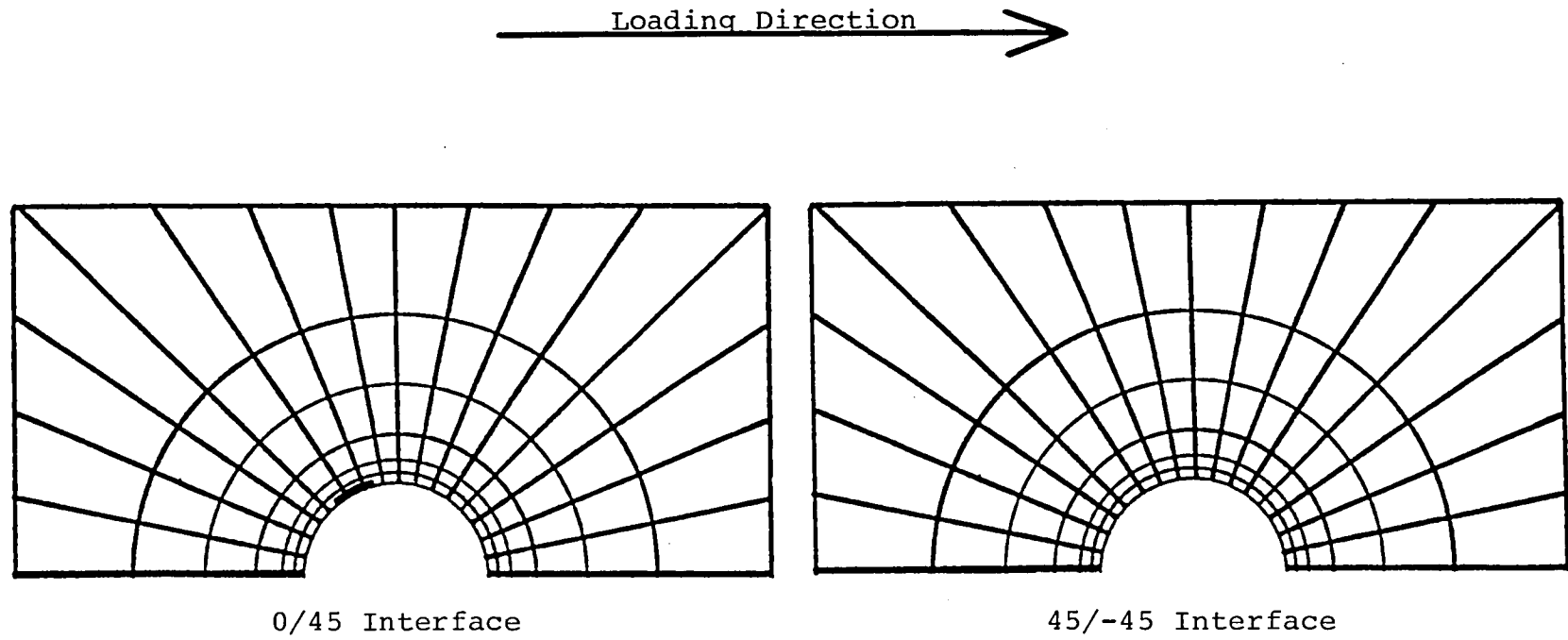
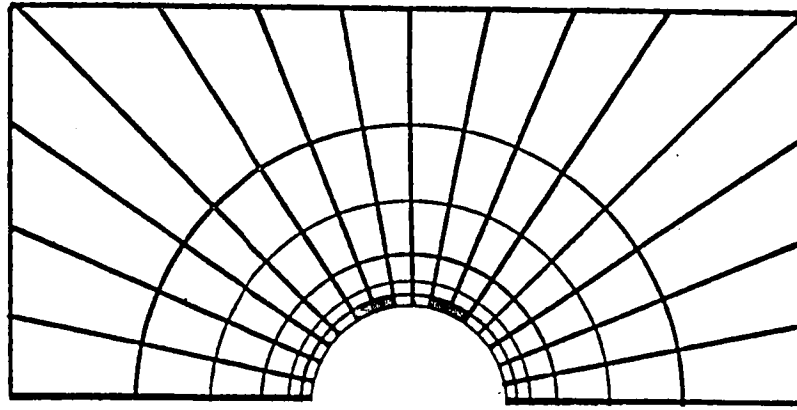
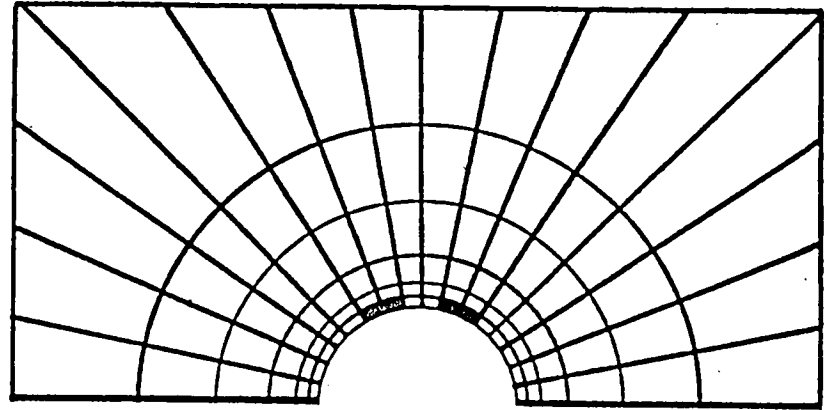



Figure 27. Interlaminar Damage at Fatigue Load, 103 MPa, $N = 1000$, in a $[0_2/\pm 45]_s$ Notched Plate

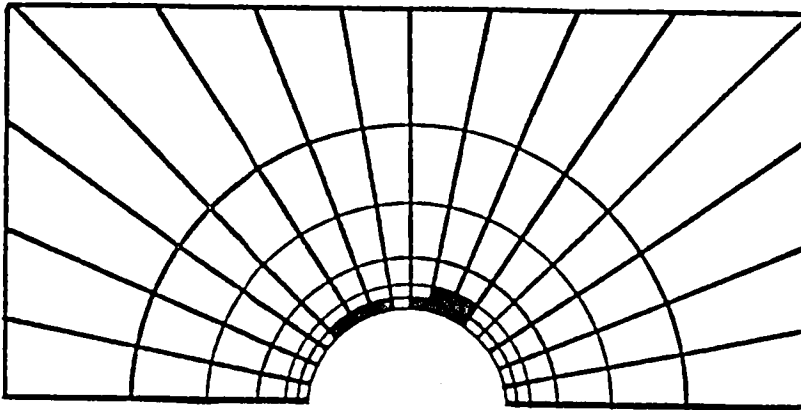


First 0° Ply

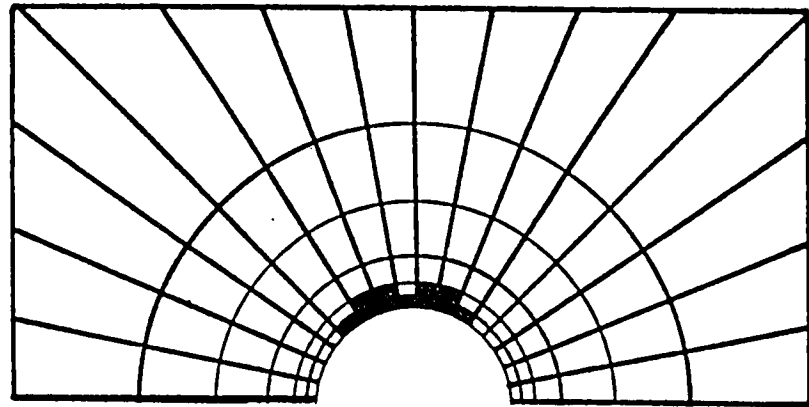


Second 0° Ply

Loading Direction 



45° Ply



-45° Ply

Figure 28. In-Plane Damage at 186 MPa, $N = 1000$, in a $[0_2/\pm 45]_S$ Notched Plate

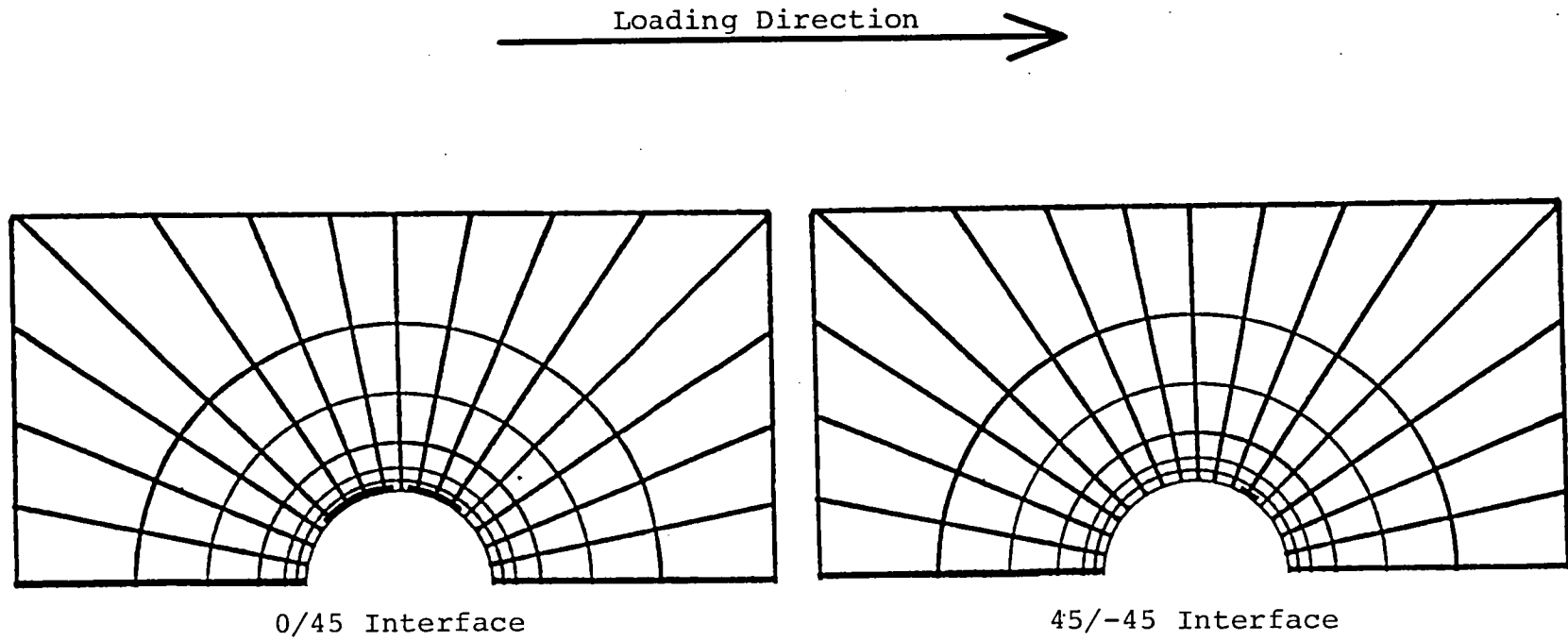


Figure 29. Interlaminar Damage at 186 MPa, $N = 1000$, in a $[0_2/\pm 45]_S$ Notched Plate

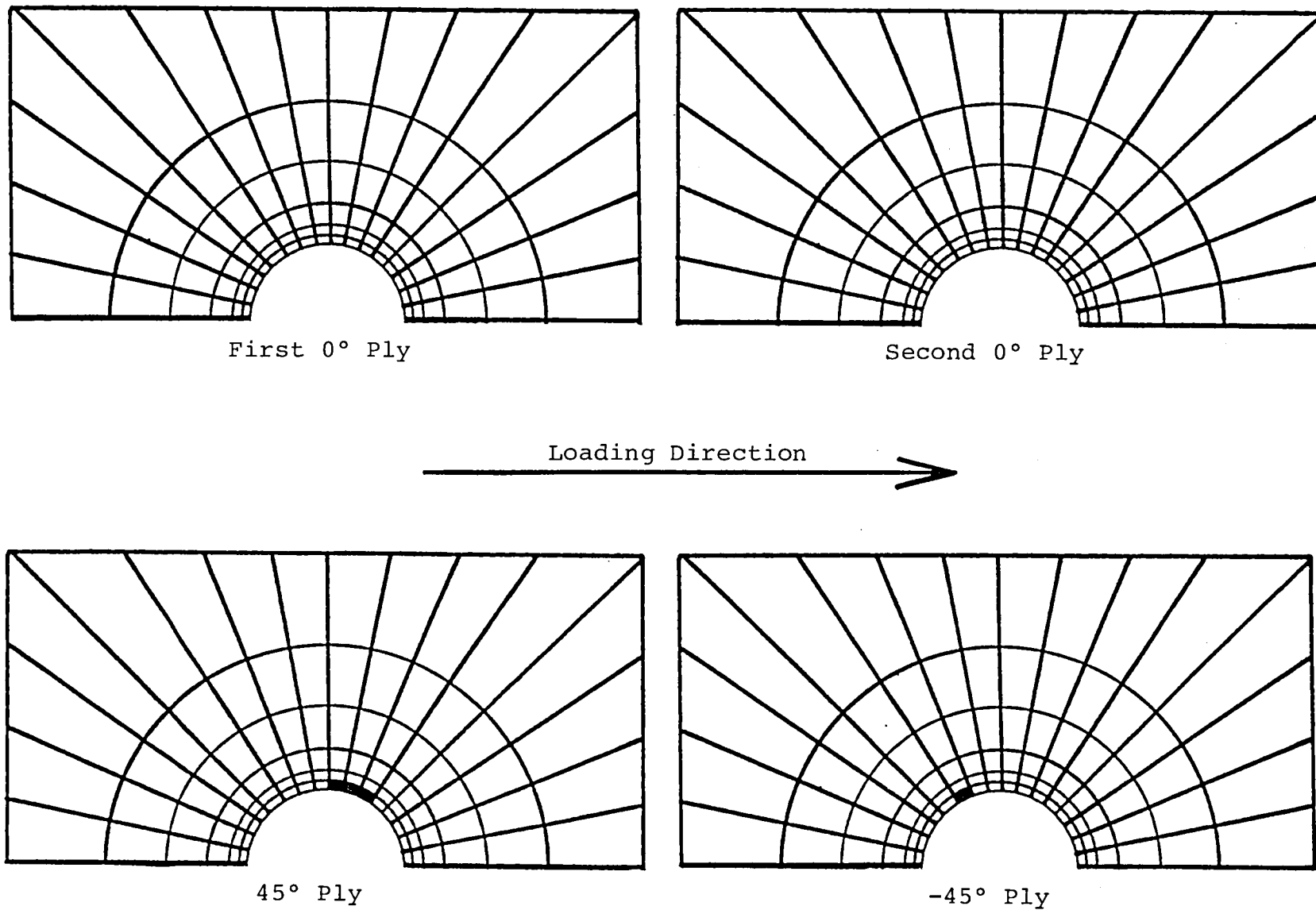


Figure 30. In-Plane Damage at the Fatigue Load, 103 MPa, $N = 10,000$, in a $[0_2/\pm 45]_S$ Notched Plate

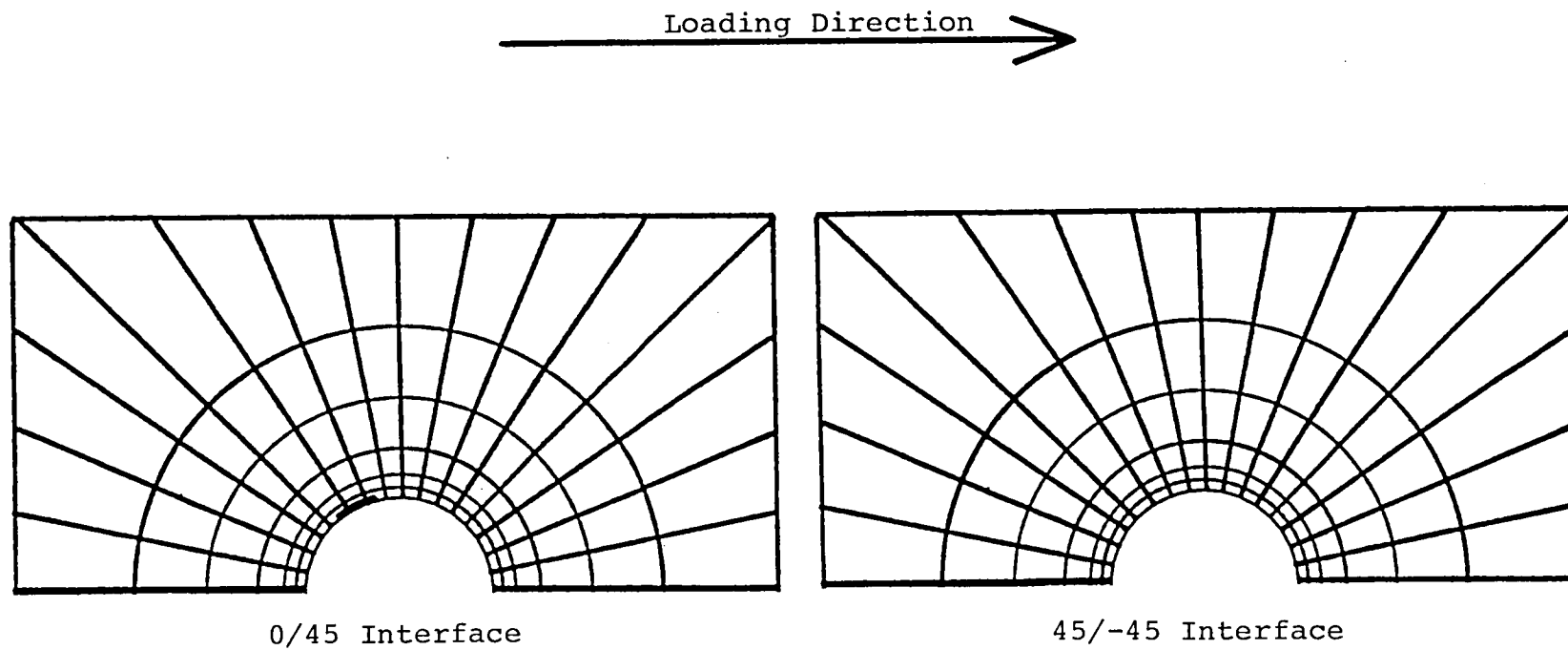


Figure 31. Interlaminar Damage at Fatigue Load, 103 MPa, $N = 10,000$, in a $[0_2/\pm 45]_s$ Notched Plate

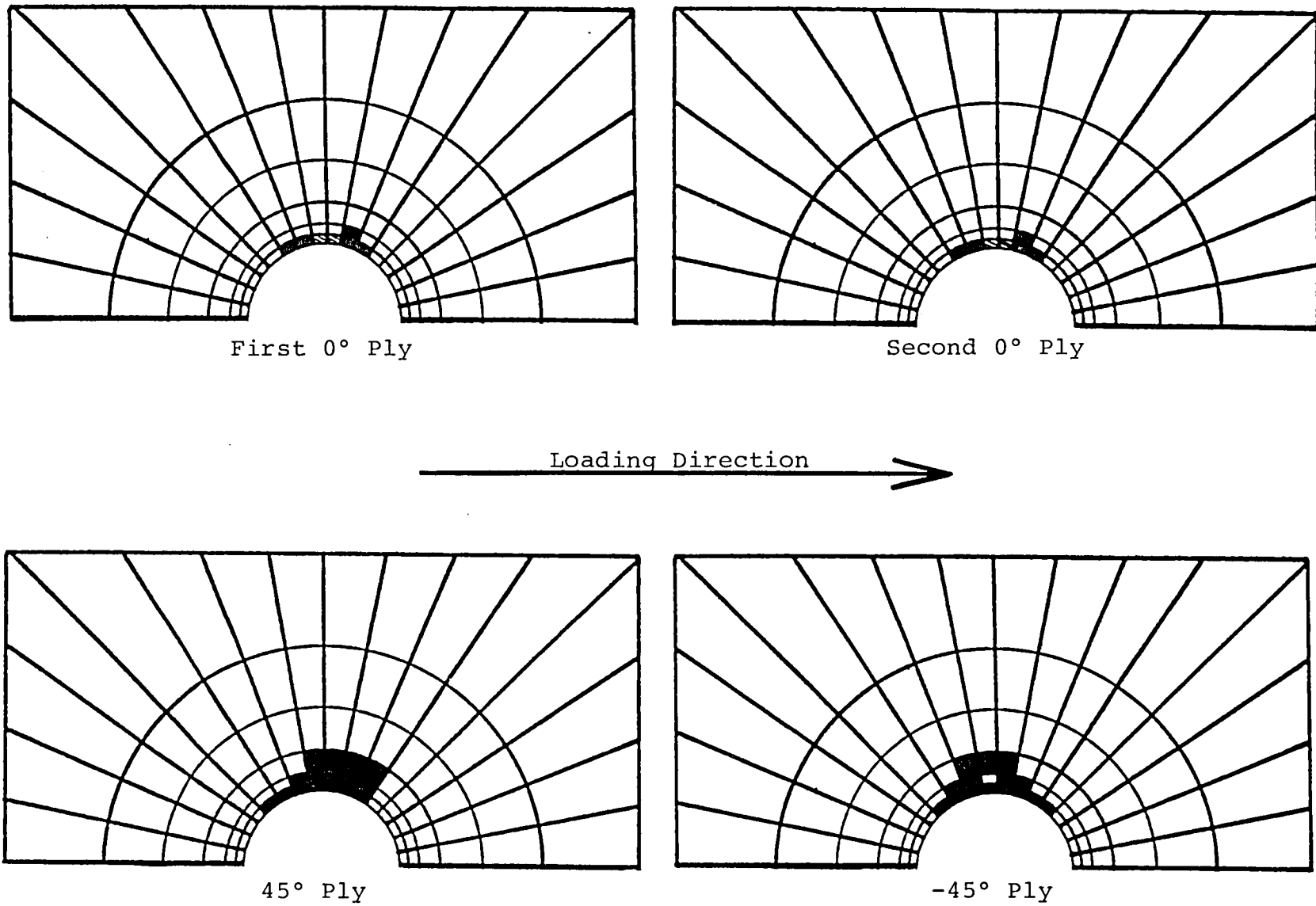


Figure 32. In-Plane Damage at 208 MPa, $N = 10,000$, in a $[0_2/\pm 45]_s$ Notched Plate

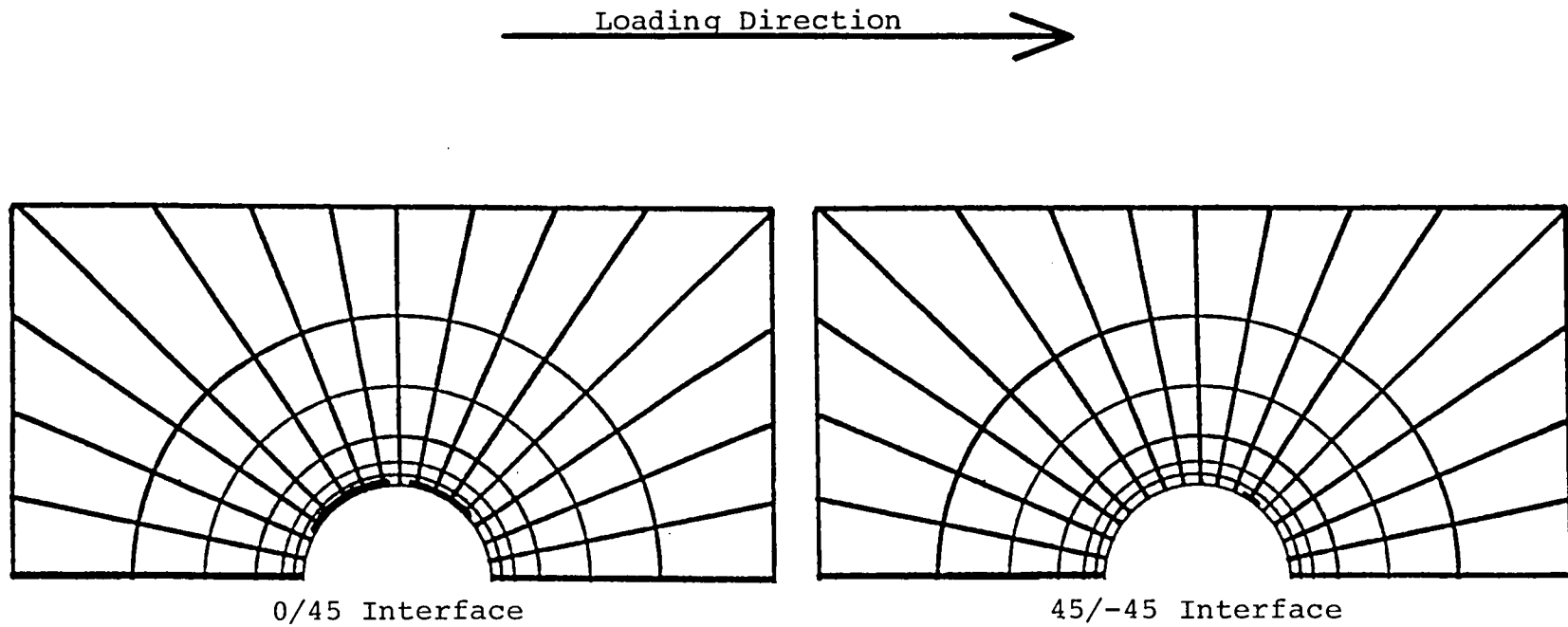


Figure 33. Interlaminar Damage at 208 MPa, $N = 10,000$, in a $[0_2/\pm 45]_S$ Notched Plate

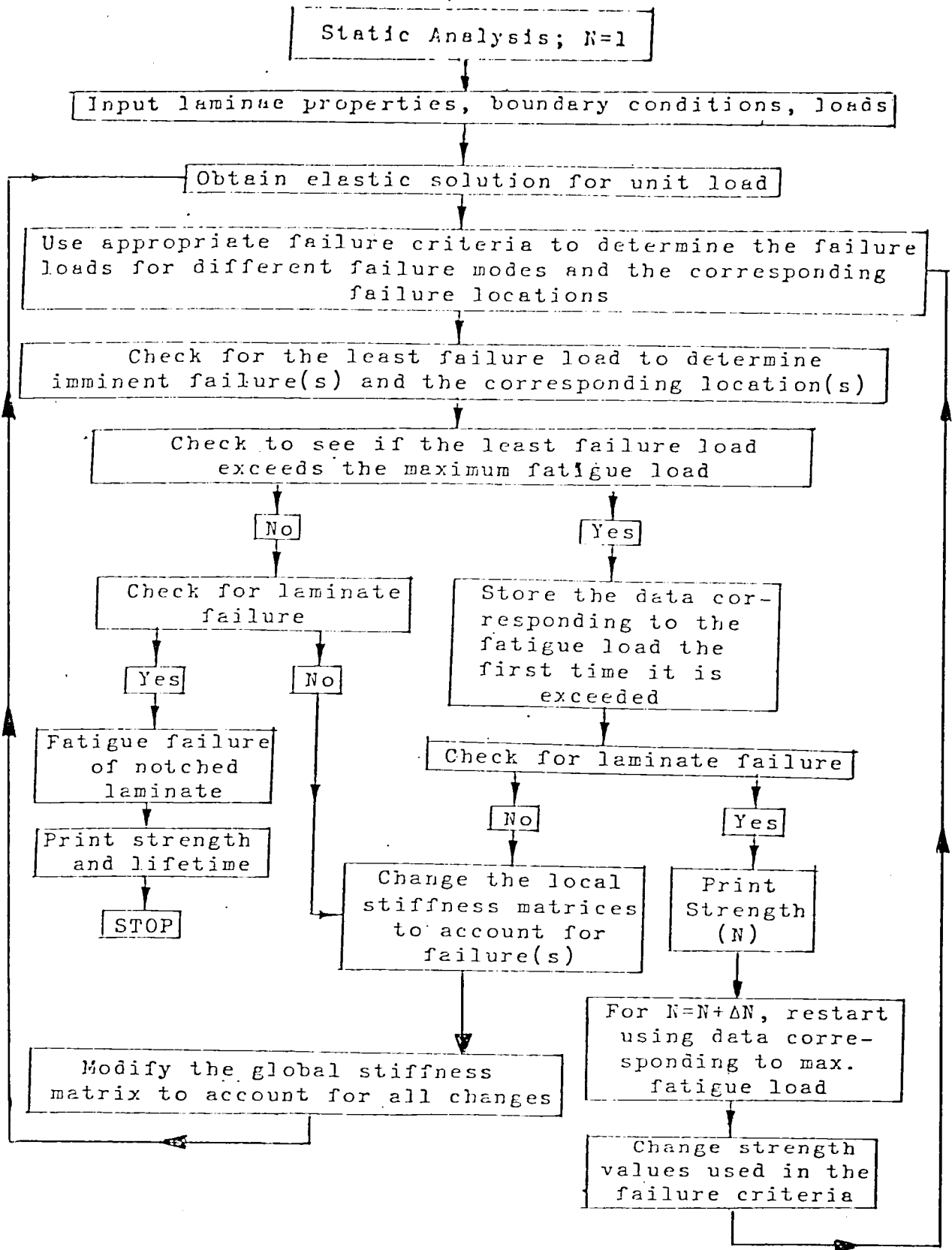


Figure A-1. Flow Chart of Computerized Fatigue Analysis Methodology

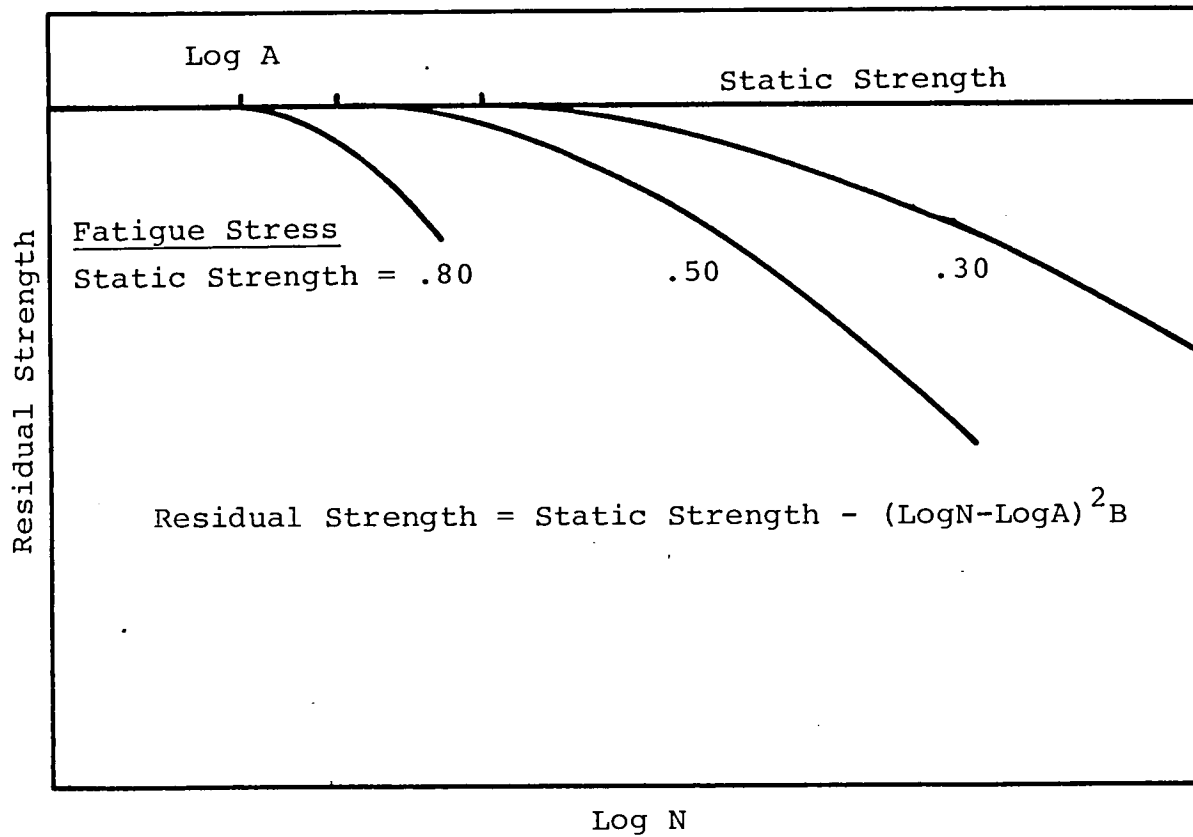


Figure A-2. Form of Lamina Residual Strength Data

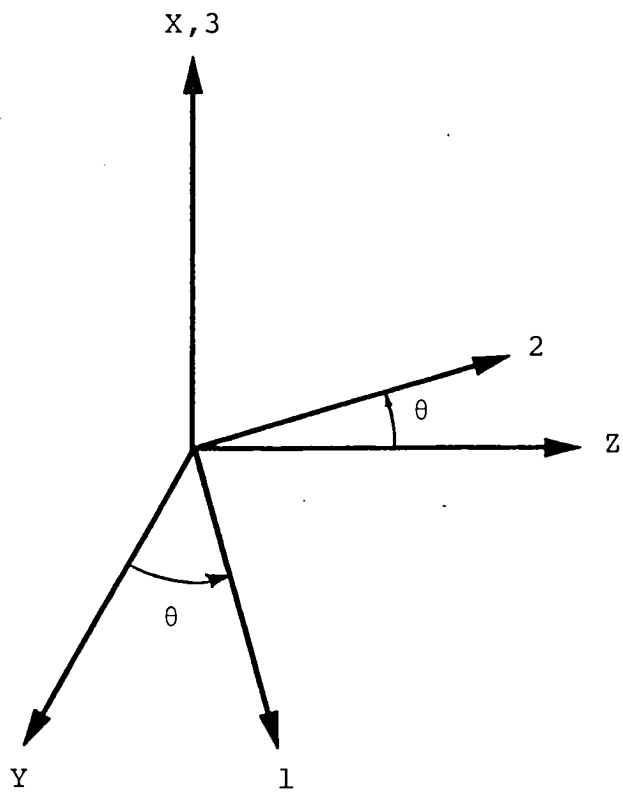


Figure A-3. FLAC Coordinate System

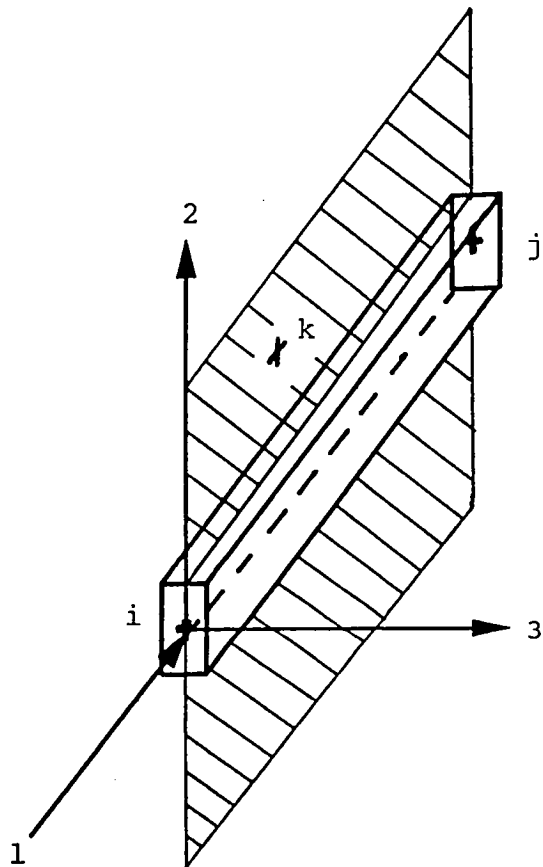


Figure A-4. Beam Node and Force Definition

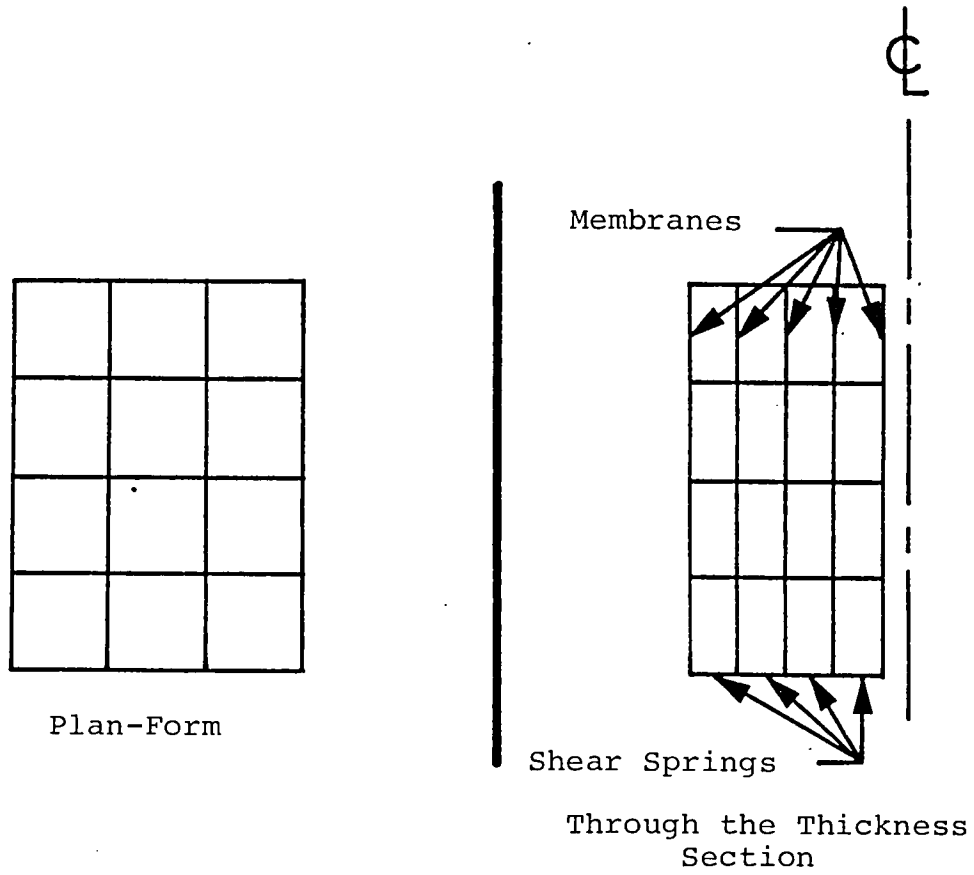
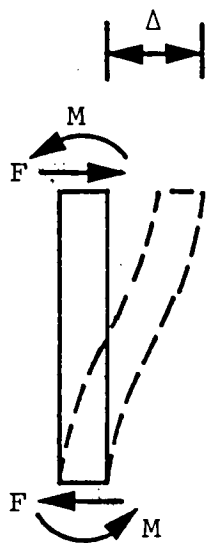
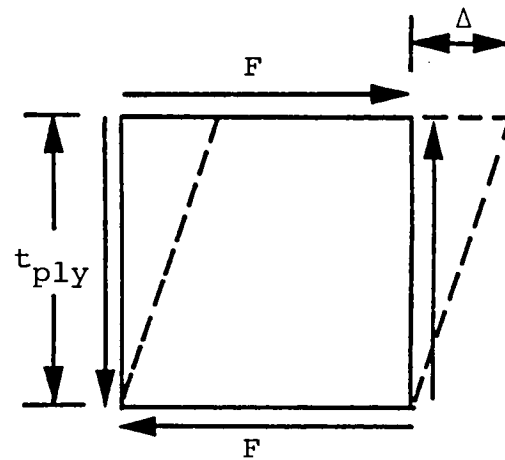


Figure B-1. Membrane and Shear Spring Model of a Balanced Symmetric Laminated Plate with Ten Plies



$$\Delta = \frac{Ft_{ply}^3}{12EI}$$



$$\Delta = \frac{Ft_{ply}}{AG}$$

$$I = \frac{AGt_{ply}^2}{12E}$$

Figure B-2. Shear Spring Stiffnesses

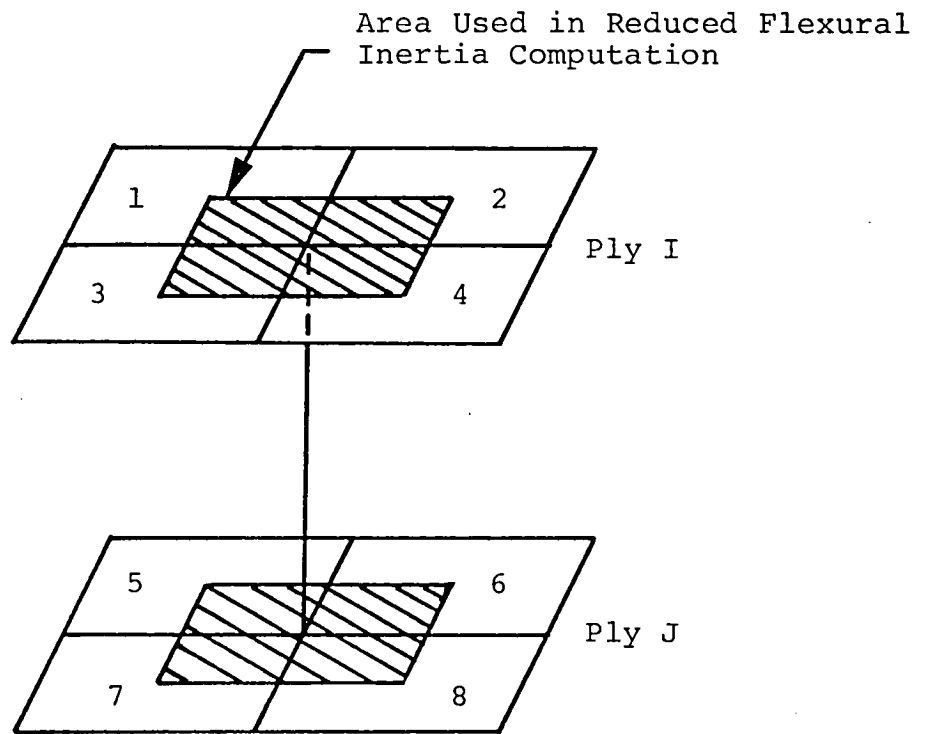


Figure B-3. Area Used in Determining Shear Spring Stiffness

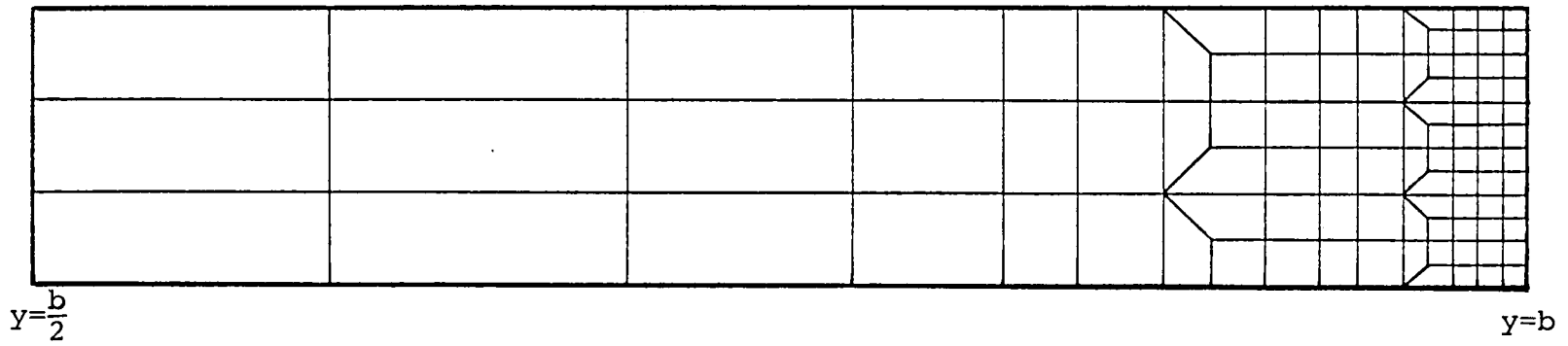
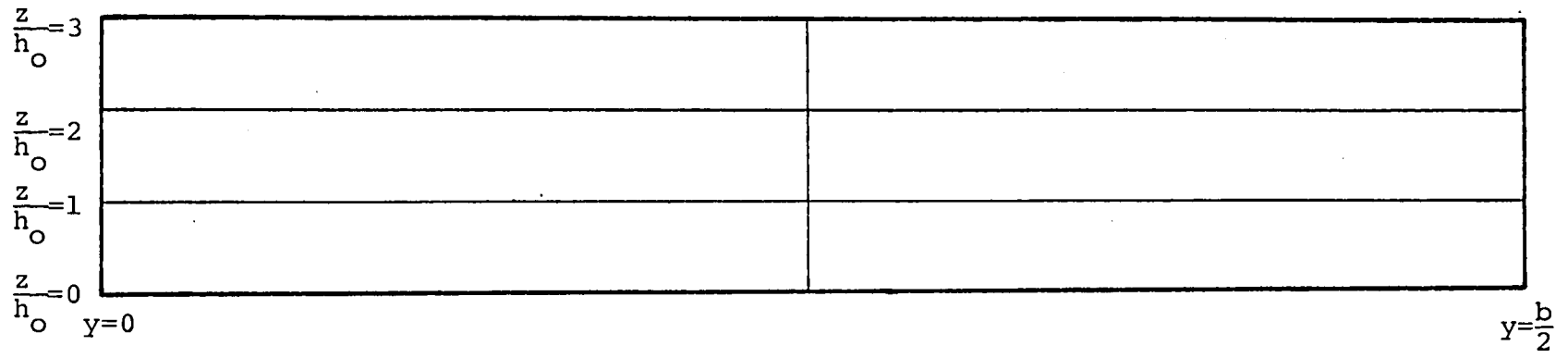


Figure C-1. Quasi Three-Dimensional Finite Element Analysis Model Geometry

NASA Contractor Report 159119
NA81-15411
DISTRIBUTION LIST

	<u>No. Copies</u>
NASA Langley Research Center Hampton, VA 23665 Attn: Report & Manuscript Control Office, Mail Stop 180A	1
Structures Laboratory, USARTL (AVRADCOM), Mail Stop 266	2
G. L. Roderick, Mail Stop 188E	21
NASA Ames Research Center Moffett Field, CA 94035 Attn: Library, Mail Stop 202-3	1
Headquarters, USARTL (AVRADCOM), Mail Stop 207-1	2
Aeromechanics Lab, USARTL (AVRADCOM), Mail Stop 215-1	2
NASA Hugh L. Dryden Flight Research Center Edwards, CA 93523 Attn: Library	1
NASA Goddard Space Flight Center Greenbelt, MD 20771 Attn: Library	1
Jet Propulsion Laboratory 4800 Oak Grove Drive Pasadena, CA 91103 Attn: Library, Mail Stop 111-113	1
NASA Lyndon B. Johnson Space Center Houston, TX 77058 Attn: JM6/Library	1
John F. Kennedy Space Center, NASA Kennedy Space Center, FL 32899 Attn: Library, IS-DOC-1L	1
NASA Lewis Research Center 21000 Brookpark Road Cleveland, OH 44135 Attn: Library, Mail Stop 60-3	1
Propulsion Lab, USARTL (AVRADCOM), Mail Stop 500-317	2
NASA George C. Marshall Space Flight Center Marshall Space Flight Center, AL 35812 Attn: Library, AS61L	1

DISTRIBUTION LIST

2
No.
Copies

National Aeronautics and Space Administration
Washington, DC 20546
Attn: RTM-6

1

University of Wisconsin
Department of Engineering Mechanics
Madison, WI 53706
Attn: Professor R. E. Rowlands

1

United Aircraft Corporation
Pratt & Whitney Aircraft
East Hartford, CT 06118
Attn: Dr. T. A. Cruse, Scientific Analysis Group

1

University of Wyoming
Department of Mechanical Engineering
Laramie, WY 82070
Attn: Professor Donald F. Adams

1

University of Minnesota
107 Aeronautical Engineering Building
Minneapolis, MN 55455
Attn: Professor Phil Hodge

1

Northrop Corporation
Aircraft Division
3901 W. Broadway
Hawthorne, CA 90250
Attn: Glen C. Grimes, Engineering Specialist,
Structures R&T, Dept. 3780/62

1

Kedwork, Kawa & Associates, Ltd.
400 Kelvin Boulevard
Winnipeg, Manitoba
Canada R3P 0J2
Attn: Dr. Keith T. Kedwork

1

McDonnell-Douglas Corporation
P. O. Box 516
St. Louis, MO 63166
Attn: Dr. Michael P. Renieri, Bldg. 34, Post 350
Dr. Gary D. Renieri, Bldg. 106, Level 4, Post C-5

1

1

Department of the Navy
Office of Naval Research
Arlington, VA 22217
Attn: Dr. Nicholas Perrone, Director, Structural Mechanics Prog.

1

DISTRIBUTION LIST

3
No.
Copies

National Science Foundation Washington, DC 20550 Attn: Dr. Clifford J. Astill, Solid Mechanics Program	1
Air Force Flight Dynamics Laboratory Wright-Patterson AFB, OH 45433 Attn: Dr. George P. Sendeckyj, Structures Division Dr. J. C. Halpin	1 1
Air Force Materials Laboratory Wright-Patterson AFB, OH 45433 Attn: Dr. J. M. Whitney, Nonmetallic Materials Division Dr. H. T. Hahn, Nonmetallic Materials Division Dr. N. J. Pagano, MBM Dr. S. Tsai, MBM	1 1 1 1
University of Delaware Department of Mechanical & Aerospace Engineering 107 Evans Hall Newark, DE 19711 Attn: Dr. R. Byron Pipes	1
Battelle-Columbus Laboratories 505 King Avenue Columbus, OH 43201 Attn: Dr. Edmund F. Rybicki	1
Lawrence Livermore Laboratory University of California Livermore, CA 94550 Attn: Dr. S. Kulkarni	1
IIT Research Institute 10 West 35 Street Chicago, IL 60616 Attn: Dr. I. M. Daniel, Manager	1
General Dynamics Corporation Fort Worth, TX 76101 Attn: M. E. Waddoups	1
McDonnell-Douglas Corporation McDonnell-Douglas Astronautics Company 5301 Bolsa Avenue Huntington Beach, CA 92647 Attn: Dr. Longin B. Greszczuk	1

DISTRIBUTION LIST

4
No.
Copies

University of Illinois
Department of Theoretical and Applied Mechanics
100E Talbot Laboratory
Urbana, IL 61801

1

Lockheed Aircraft Corporation
Lockheed-California Company
P. O. Box 551
Burbank, CA 91520
Attn: Larry R. Markham, Dept. 7572, Bldg. 63, Plant A1

1

The Boeing Company
P. O. Box 3707
Seattle, WA 98124
Attn: John McCarty, Mail Stop 30-01

1

Applied Technology Laboratory, USARTL (AVRADCOM)
Fort Eustis, VA 23604
Attn: J. Robinson/SAVDL-EU-SS
A. J. Gustafson

1

1

Department of the Army
U.S. Army Materials & Mechanics Research Center
Watertown, MA 02172
Attn: Dr. E. Leno
Dr. J. Perkins

1

1

Picatinny Arsenal
Materials Engineering Laboratory, Bldg. 183
Dover, NJ 07801
Attn: Charles Wright

1

Naval Air Development Center
Warminster, PA 18974
Attn: Dr. Jim Huang, Code 3033

1

NASA Scientific & Technical Information Facility
6571 Elkridge Landing Road
Linthicum Heights, MD 21090

30
plus original

